Exploring Spontaneous Visual-Spatial Memory Reactivation During Slow-Wave Sleep Using Multi-Voxel Pattern Analysis

M.Sc. Thesis

Qin Ding

Integrated Program in Neuroscience

McGill University, Montreal

August 2024

Table of Contents

Abbreviations

Area Under the Curve (AUC)

Blood Oxygenation Level Dependent (BOLD)

Default Mode Network (DMN)

Electroencephalogram (EEG)

Functional Magnetic Resonance Imaging (fMRI)

Hemodynamic Response Function (HRF)

Multi-voxel Pattern Analysis (MVPA)

NREM Sleep, Stage 1 (N1)

NREM Sleep, Stage 2 (N2)

NREM Sleep, Stage 3 (N3)

Non-Rapid Eye Movement Sleep (NREM)

Rapid Eye Movement (REM)

Receiver Operating Characteristic (ROC)

Support Vector Machines (SVM)

Slow Oscillations (SOs)

Slow-wave Activity (SWA)

Slow-wave Sleep (SWS)

Exploring Spontaneous Visual-Spatial Memory Reactivation During Slow-Wave Sleep Using Multi-Voxel Pattern Analysis

Abstract

Introduction

Based on the active system consolidation hypothesis, memory reactivation during slow-wave sleep (SWS) facilitates the transfer of memory representations from the hippocampus to cortical brain regions. Support for this hypothesis stems from studies demonstrating that rodents' hippocampus cells replay in the same sequence during sleep as during prior awake running tasks. While numerous human studies support the role of SWS in offline declarative memory consolidation, direct evidence of memory reactivation during SWS remains elusive. Visual-spatial memory, involving the participation of multiple brain regions (especially the hippocampus and cortical areas associated with memory retrieval and visual perception), offers a solution for displaying complex patterns in the brain that are activated by memory. This study utilizes multi-voxel activation patterns of visual-spatial memory to investigate the characteristics of memory activation during sleep, specifically focusing on SWS, thereby providing empirical support for the active system consolidation hypothesis.

Hypothesis

We hypothesize that brain patterns resembling memory recognition during wakefulness preferentially reactivate during SWS compared to other sleep stages.

Methods

This study enrolled 11 healthy adults (mean age = 21.55 ± 1.78) to participate in the experiment. After completing the encoding and location-object context memory retrieval tasks, participants slept and then proceeded with a combination of memory retrieval and recognition tasks. Synchronous fMRI-EEG data were collected during sleep, and fMRI data were collected during tasks before and after sleep. Ultimately, 7 participants entered SWS sleep and were included in the final analysis.

A machine learning model was used to identify memory reactivation in sleep by employing multi-voxel pattern analysis (MVPA) to fMRI data of visual-spatial memory tasks and sleep stages. The fMRI dataset for training the model includes HIT and CORRECT REJECTION labels derived from behavioral classifications in the old-new item memory task. At the same time, REST represents the wake-resting state at the beginning of the sleep scan. HIT is indicative of memory activation mode for the target, whereas the other two represent control modes for different states. The model was trained within each subject. Each sample's feature vector was filtered through a mask defined by the ANOVA-SVM method and classified using a Support Vector Machine (SVM) classifier. The performance and interpretability of the model were proved. After validation, the model was applied to sleep fMRI data to predict the likelihood of each volume being one of the three states.

Results

There is a higher likelihood of the REST state before sleep onset and HIT and CORRECT REJECTION states after sleep onset. This aligns with the hypothesis and supports the applicability of the constructed model. Four out of seven participants showed greater HIT likelihood during SWS compared to CORRECT REJECTION. HIT scores during SWS were significantly higher than during the Wake stage of sleep, confirming prioritized reactivation of visual-spatial memory during SWS. Interestingly, a high HIT score was also observed during N2 sleep. Additionally, changes in memory performance before and after sleep negatively correlated with HIT during wakefulness, suggesting that wakeful reactivation may hinder memory consolidation. In conclusion, this exploratory study supports the active system consolidation framework by providing direct evidence that memory recognition patterns are specifically reactivated during SWS sleep and adding details to the framework.

Résumé

Introduction

Selon l'hypothèse de consolidation active du système, la réactivation de la mémoire pendant le sommeil à ondes lentes (SWS) facilite le transfert des représentations mnésiques de l'hippocampe vers les régions corticales. Cette hypothèse est soutenue par des études où les cellules de l'hippocampe des rongeurs rejouent la même séquence pendant le sommeil que lors de tâches effectuées à l'état d'éveil. Bien que des études humaines appuient le rôle du SWS dans la consolidation de la mémoire déclarative, des preuves directes de la réactivation mnésique pendant le SWS sont rares. La mémoire visuo-spatiale, qui implique la participation de plusieurs régions cérébrales (en particulier l'hippocampe et les zones corticales associées à la récupération mnésique et à la perception visuelle), offre une solution pour représenter les motifs complexes activés dans le cerveau par la mémoire. Cette étude utilise des motifs d'activation multi-voxel pour étudier l'activation mnésique pendant le SWS, fournissant un soutien empirique à l'hypothèse de consolidation active du système.

Hypothèse

Nous émettons l'hypothèse que les motifs cérébraux ressemblant à la reconnaissance mnésique pendant l'éveil se réactivent préférentiellement pendant le SWS par rapport aux autres phases du sommeil.

Méthodes

Onze adultes en bonne santé (âge moyen = 21,55 ± 1,78) ont participé à l'étude. Après avoir réalisé des tâches d'encodage et de récupération de la mémoire dans le contexte lieu-objet, les participants ont dormi, puis ont effectué des tâches de récupération et de reconnaissance. Des données fMRI-EEG synchrones ont été collectées pendant le sommeil, ainsi que des données fMRI pendant les tâches avant et après le sommeil. Finalement, 7 participants ayant atteint le SWS ont été inclus dans l'analyse finale.

Un modèle d'apprentissage automatique a été utilisé pour identifier la réactivation mnésique pendant le sommeil en appliquant l'analyse de motifs multi-voxel (MVPA) aux données fMRI des tâches visuo-spatiales et des phases de sommeil. Le modèle a été entraîné pour chaque sujet individuellement. Le vecteur de caractéristiques de chaque échantillon a été filtré à travers un masque défini par la méthode ANOVA-SVM et classé à l'aide d'un classificateur SVM (Support Vector Machine). Les étiquettes HIT et CORRECT REJECTION, dérivées des classifications comportementales dans la tâche de mémoire des éléments anciens-nouveaux, ont été utilisées pour l'entraînement du modèle. Parallèlement, REST a été utilisé pour représenter l'état de repos-éveil au début de l'examen du sommeil. HIT indique l'activation mnésique, tandis que les autres états servent de contrôles. La performance et l'interprétabilité du modèle ont été validées. Ensuite, le modèle a été appliqué aux données fMRI du sommeil pour prédire la probabilité de chaque volume d'appartenir à l'un des trois états.

Résultats

L'état REST est plus probable avant l'endormissement, tandis que HIT et CORRECT REJECTION sont plus probables après. Quatre participants sur sept ont montré une probabilité de HIT plus élevée pendant le SWS par rapport à CORRECT REJECTION. Les scores de HIT pendant le SWS étaient significativement plus élevés que pendant l'éveil, confirmant la réactivation prioritaire de la mémoire visuo-spatiale pendant le SWS. Un score HIT élevé a également été observé pendant le sommeil N2. De plus, les changements dans la performance mnésique avant et après le sommeil étaient négativement corrélés avec HIT pendant l'éveil, suggérant que la réactivation à l'éveil pourrait entraver la consolidation mnésique. En conclusion, cette étude soutient l'hypothèse de consolidation active du système en apportant des preuves directes de la réactivation des motifs mnésiques pendant le SWS, tout en précisant ce cadre.

Acknowledgments

First and foremost, I would like to express my sincere gratitude to my supervisors, Dr. Xiaoqian Chai, Dr. Reut Gruber, and Dr. Tiejun Liu for providing me with invaluable guidance, direction, and support throughout my training and research. I thank them for their open arms and trust in my ability, and for giving me the greatest support in what they are good at. I feel very lucky to have these mentors.

I would like to thank senior PhD student Lin Wang for helping me throughout the M.Sc. study. He taught me many basic concepts, theories, and methods of scientific research. In the process of this project, he always supported me and solved many practical difficulties. Thanks to Mao qin Peng and Shuo Chen for their inspiration and help to me in the field of fMRI principles and the MVPA method, which is essential to this thesis. I would like to thank other lab mates, Jonah Kember, Honxiu Jiang, Hilary Sweatman, Ying He, and Paula Toro Vargas for enthusiastically providing their views and answering my questions in the lab meetings.

Thanks to my committee members Dr. Marc Roig Pull and Dr. Signy Sheldon for following the progress of this project and providing me with key revision suggestions. Thanks to my mentor Julien Doyon for his resources and help when I was having trouble with my project.

In addition, thank you to McGill University's Integrated Program in Neuroscience (IPN) for giving me the opportunity to join their research community. Thanks to Mengting Hu and Dr. Edward Ruthazer for their reminders and explanations on every study milestone.

Finally, thank you to friends and family for their continued support and encouragement throughout my academics. Best wishes to everyone I acknowledged.

Contributions of Authors

As the lead author of this original and independent thesis, I initiated the experiment, processed neuroimage data, and designed the MVPA script. I interpreted the findings, generated the figures, and wrote the thesis. Lin Wang participated in the experimental design, processed and staged EEG data together with Yahui Zhao. Geng Liu and Huiling Jiang assisted with the data collection. Maoqin Peng taught me the fMRI preprocessing method. Ying He and Paula Toro Vargas reviewed this thesis. Dr. Xiaoqian Chai designed the master's project, developed the research questions, guided the research method, and supervised this project. Dr. Reut Gruber and Dr. Tiejun Liu co-supervised the master's project and advised on research questions and thesis writing. Dr. Tiejun Liu financed the experiment.

List of Figures

List of Tables

Exploring Spontaneous Visual-Spatial Memory Reactivation During Slow-Wave Sleep Using Multi-Voxel Pattern Analysis

Introduction

Philosopher Plato once said (Ebrahimi, 2021), "Learning is remembering. " Long-term memory is a crucial cognitive ability, serving as a bridge between humanity's past, present, and future. Meanwhile, sleep, occupying one-third of life, is a vital human activity. Extensive research has confirmed the irreplaceable role of sleep in long-term memory (Brodt, Inostroza, Niethard, & Born, 2023; Denis & Cairney, 2023; Klinzing, Niethard, & Born, 2019). Background memory and sleep knowledge related to this study will be introduced in this chapter, as well as the relationship between sleep and memory consolidation. Specifically, the focus will be on visual-spatial memory and slow-wave sleep (SWS), including the current research status of memory reactivation during SWS. Additionally, the application of Multi-voxel Pattern Analysis (MVPA) in memory reactivation will be introduced. Finally, based on the existing research gap regarding memory replay during human SWS, the research question, hypothesis, and research approach for this study will be proposed.

Memory

Categories of Memory

According to the length of time that information remains available to us, memory is typically categorized into sensory memory, short-term memory, and long-term memory (Votaw, 2023). Sensory memory involves the direct storage of sensory information, enabling future accessibility of this information (Tripathy & Öğmen, 2018). Short-term memory encompasses the processing and storage of a small amount of information over a short period (Baddeley, 1990). Long-term memory allows for the storage of information over extended periods (Brodziak, Brewczyński, & Bajor, 2013). Through rehearsal and encoding, the storage of information moves from one stage to the next, from sensory to short-term

and then to long-term memory (Miller & Cohen, 2001).

When talking about remembering something, people often refer to long-term memory (Fig 1.1). Long-term memory can be classified into declarative memory and non-declarative memory (Squire & Dede, 2015). Declarative memory, also known as explicit memory, involves the storage and retrieval of facts, concepts, and events that can be consciously expressed. It comprises two subtypes: episodic memory and semantic memory. Episodic memory refers to personal experiences with details of time and place, such as the first day of school, or a friend's birthday party (Dickerson & Eichenbaum, 2010). Semantic memory, which encompasses general knowledge and objective facts about the world, is based on long-term personal experiences, such as word definitions.(Kolb & Whishaw, 2009). Non-declarative memory, on the other hand, is implicit and inexpressible. It includes procedural skills, the priming effect, associative learning, and non-associative learning (Slotnick, 2017).

Figure 0.1. Categories of long-term memory, adapted from Slotnick (2017)

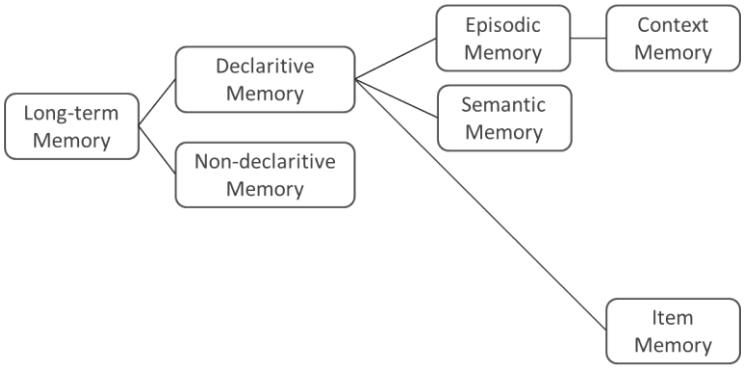

Note. Long-term memory is categorized into declarative memory and non-declarative memory based on whether consciousness is involved. Within declarative memory, episodic memory vs. semantic memory, and item memory vs. context memory are two complementary concepts.

Item Memory and Context Memory

Item memory and context memory are straightforward terms that refer to different kinds of memory that operate during context memory experiments (e.g. Ladenbauer et al., 2017; Wang, Weber, Zinke, Noack, & Born, 2017). In these experiments, items are paired with contextual information during

the study phase, such as associating a word (item) with a picture or a specific position on a screen (context). During the test phase, item memory involves determining whether the item is old or new, or whether it belongs to the first or second group. In contrast, context memory involves recalling the background information associated with the item (e.g., position 1 or position 2). Different memory processes are engaged during the assessment of item and context memory. Item memory relies on recognition, which involves correctly identifying whether an item belongs to one of two categories, representing a judgment of "Yes or No" regarding a particular event (Weymar, Ventura-Bort, Wendt, & Lischke, 2019). In contrast, context memory relies on familiarity with previous contextual information, typically used to trace the origins of a particular event (Buck, Bastos, Baldeweg, & Vargha-Khadem, 2021).

Visual-spatial Memory

Visual-spatial memory is a type of declarative memory that corresponds to the ability to recognize object features and identify object locations in the environment(McAfoose & Baune, 2009). The visual-spatial function involves the ability to locate small parts within an overall shape (context memory) or to discern differences and similarities between objects (item memory; Li, 2021). Visual-spatial abilities are used for ordinary use from navigation, sympathetic or fixing equipment, sympathetic or estimating distance and dimension, and performing on a job (Babu & Ganesan, 2020).

The brain areas or circuits associated with memory reactivation are involved in the entire process of memory encoding, consolidation, and retrieval. Brain regions related to visual-spatial memory include the visual cortex, which is where visual perception originates. The parietal cortex (PC) is associated with directed attention towards targets(Rolls, Deco, Huang, & Feng, 2022), where the intraparietal sulcus (IPS) is involved in the dorsal visual pathway, processing spatial information within objects(Swisher, Halko, Merabet, McMains, & Somers, 2007; Ayzenberg & Behrmann, 2022), and the precuneus plays a role in memory retrieval (Flanagin et al., 2023). The posterior parietal cortex (PPC) is

closely associated with overall spatial perception (Kesner, 2009). The prefrontal cortex (PFC) exerts top-down control over encoding, with the ventrolateral prefrontal cortex (VLPFC) involved in the semantic processing of memory representations, and the dorsolateral prefrontal cortex (DLPFC) engaged in selection, manipulation, and organization (Goldman-Rakic, 1996; Romanski, 2004). In processing declarative memory information, the medial temporal lobe (MTL) is involved in binding items and spatial information, particularly the hippocampus and perirhinal cortex (Diana, Yonelinas, & Ranganath, 2007). To summarize, visual-spatial memory engages multiple brain regions, and studying the replay of spatial-visual memory is best approached from the perspective of whole-brain patterns.

Figure 0.2. Object-location Associative Memory Task Paradigm

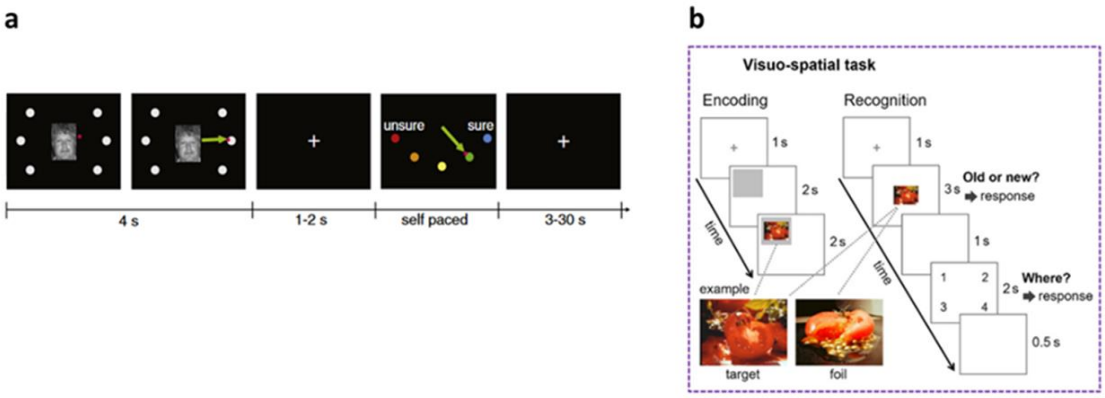

Note. (a) Dongen et al. (2011) utilized a paradigm where different faces were associated with 6 specific locations, with participants rating their confidence in memory retrieval on a scale from 1 to 5. (b) Ladenbauer et al. (2017) introduced enhancements to the object-location pairing task by incorporating an old-new item recognition task. Participants were required to identify images of the same type but with subtle differences after the object-location pairing test, thus augmenting the spatial-visual memory task with an additional item memory component.

The object-location associative memory task is a paradigm used to assess human visual-spatial memory. It requires participants to associate images displayed on a screen with specific indicated positions on the screen. Originally used in short-term memory studies (with a delay between encoding and recall of 4-8 minutes; Milner, Johnsrude, & Crane, 1997), this paradigm has also been applied to

long-term memory research in recent years (Fig. 1.2).

Sleep

Sleep Stages

Human sleep is typically divided into two main stages: REM (Rapid Eye Movement) sleep and non-REM sleep (Fig 1.3); non-REM sleep consists of three stages: N1, N2, and N3 (Iber, Ancoli-Israel, Chesson, & Quan, 2007). As a person transitions into sleep, the W (wake) state characterized by low-voltage fast brainwave patterns gradually gives way to slower frequencies, as non-REM sleep progresses from stage N1 (reduced alpha activity) to stage N2 (marked by sleep spindles and K-complexes), and finally to stage N3 (characterized by increased amplitude and regularity of delta waves; Nayak & Anilkumar, 2024). Following non-REM sleep, the next stage is REM sleep, characterized by rapid eye movement, during which dreaming typically occurs (Blumberg, Lesku, Libourel, Schmidt, & Rattenborg, 2020).

Figure 0.3. A Typical Full-Night Sleep Architecture

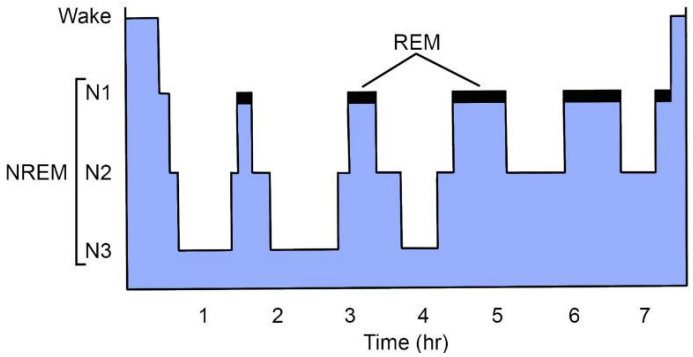

Note. After falling asleep, a sleep cycle usually goes through three stages of non-rapid eye movement (NREM) sleep, followed by a rapid eye movement (REM) stage. It usually takes 90 to 120 minutes to complete all four stages of the cycle, after which the cycle begins again. Adults typically experience four to six cycles each night(“Stages of Sleep,” 2021). As the stages of sleep progress through, the depth of sleep gradually increases and N3 is the deepest period of non-REM sleep (A. K. Patel, Reddy, Shumway, & Araujo, 2024). N3 sleep occupies a larger proportion of the first half of the night, while REM sleep predominates in the second half of the night

(Keenan & Hirshkowitz, 2017).

Slow-wave Sleep and Relative Oscillations

Slow-wave sleep (SWS) in human research is generally directly defined as non-REM sleep stage 3 (N3 sleep; Herberger et al., 2024; Höller, Eyjólfsdóttir, Van Schalkwijk, & Trinka, 2024). SWS is characterized by distinct oscillations observed in electroencephalogram (EEG) and local field potential (LFP) recordings (Staresina, Niediek, Borger, Surges, & Mormann, 2023).

The primary hallmark of SWS is the presence of sustained slow-wave activity (SWA), which manifests as high-voltage (>75 μV) synchronized waveforms comprising delta oscillations (1–4 Hz) and slow oscillations (SOs) (<1 Hz; Léger et al., 2018). SWA is the result of collective activity among cortical neurons, occurring as the neural network alternates between the DOWN state of synchronous hyperpolarization and the UP state of synchronous depolarization in approximately one-second cycles (Adamantidis, Gutierrez Herrera, & Gent, 2019). SWA originates from cortical networks (specifically layers 2/3 and 5) and predominantly propagates from anterior to posterior regions, as well as to subcortical structures including the hippocampus (Massimini, Huber, Ferrarelli, Hill, & Tononi, 2004; Nir et al., 2011; Wierzynski, Lubenov, Gu, & Siapas, 2009).

The second hallmark of SWS is the spindle. Spindles are transient, choppy oscillations with variable amplitude (peaking at 100μV), occurring at frequencies of 11-15 Hz, and lasting for 0.5-2.0 seconds with about 6-15 cycles (Fernandez & Lüthi, 2020). They originate in the thalamus due to interactions between the thalamic reticular nucleus (TRN) and other thalamic nuclei (Adamantidis et al., 2019). Spindle waves propagate throughout the neocortex via the thalamocortical circuit and extend to the hippocampus (Varela, Kumar, Yang, & Wilson, 2014). Unlike SOs, spindle wave generation primarily involves more localized networks within the neocortex (Staresina et al., 2023). Electrically induced spindle wave discharge patterns promote long-term synaptic potentiation (LTP) in cortical neurons (Rosanova & Ulrich, 2005). This increase may be achieved through elevated intracellular calcium

concentrations, as indicated by increased local calcium activity in the apical dendrites of rat cortical pyramidal cells during spindle wave periods (Almeida-Filho, Queiroz, & Ribeiro, 2018; Rosanova & Ulrich, 2005). In summary, spindle waves represent one of the candidate mechanisms for the construction of long-term representations in cortical networks.

The third hallmark of SWS is sharp-wave ripples (SWRs). SWRs comprise aperiodic transient field potentials known as sharp waves, overlaid with rapid periodic oscillations at frequencies of 150-200 Hz called ripples (Girardeau, Benchenane, Wiener, Buzsáki, & Zugaro, 2009). SWRs originate in the hippocampal-cortical reactivation hippocampus and coordinate interactions between the hippocampus and cortex (Buzsáki, 2015; Oliva, Fernández-Ruiz, Buzsáki, & Berényi, 2016). The main function of SWRs appears to be related to the temporal sequence of reactivation of hippocampal CA1 neurons, with reactivation spreading from there to the entorhinal cortex, striatum, and cortex(Malerba & Bazhenov, 2019). Ripple activity detected in cortical regions may reflect this coordinated hippocampal-cortical reactivation(Rothschild, Eban, & Frank, 2017). Therefore, SWRs are believed to play a crucial role in consolidating memory traces within the hippocampus and transferring previously acquired information from the hippocampus to the neocortex, particularly the frontal and associational cortices(Inostroza & Born, 2013; Sadowski, Jones, & Mellor, 2016).

The coupling relationship between SWA, spindles, and SWRs is a critical feature because these components typically occur in precise temporal coordination during SWS (Fig. 1.4; Klinzing et al.,2019). Studies have increasingly shown that memory consolidation is controlled by the complex interaction of three oscillations that drive synapses in a controlled manner for system integration. Ripples accompanying ensemble reactivations in hippocampal networks nest into the excitable troughs of the spindle oscillation (Azimi, Alizadeh, & Ghorbani, 2021; Jiang, Gonzalez-Martinez, & Halgren, 2019). Spindles themselves are nested in the excitable UP state of the neocortical SOs (Mikutta et al., 2019; Silversmith, Lemke, Egert, Berke, & Ganguly, 2020).

Figure 0.4. Triple-coupling of Oscillations during SWS

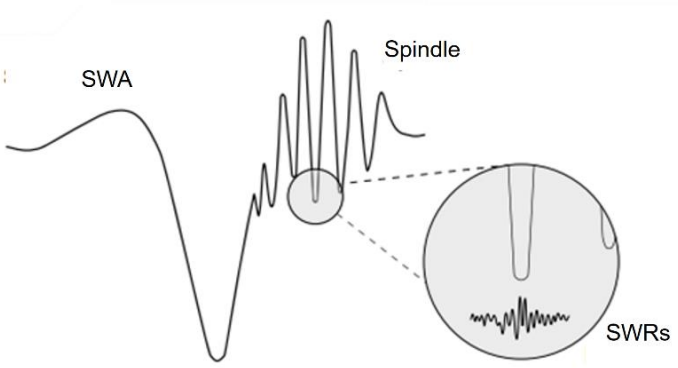

Sleep and Long-term Memory

Active System Consolidation (ASC)

Figure 0.5. Cooperation of the Three Oscillations in the ASC

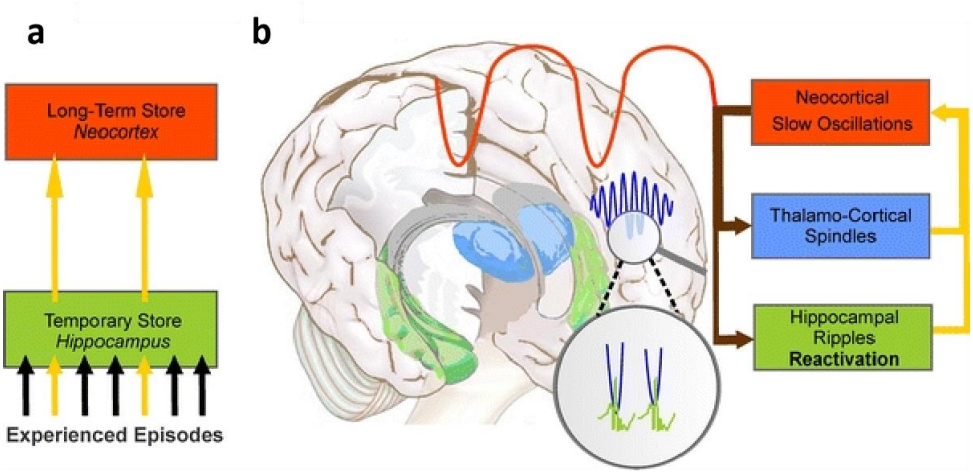

Note. (a) During SWS, newly encoded memories in the temporary storage area (hippocampus) are reactivated and reassigned to the long-term storage area (i.e., neocortex). (b) The system consolidation during SWS depends on the information exchange between the cortex and the hippocampus, which is controlled by the SOs (red) of the neocortex from above. The depolarizing UP phase of the SOs is synchronized with the hippocampal sharp waves (green) and thalamocortical reticular waves (blue), driving the repeated reactivation of hippocampal memory representations. This synchronized drive can form spindle-ripple events, in which the hippocampal sharp waves and related reactivated memory information are nested within a single trough of the spindle. Figure from Staresina, 2024.

The ASC framework (Fig. 1.5) primarily applies to long-term associative memories involving the hippocampus, proposing that memory reactivation during SWS facilitates the transfer and consolidation of memory representations between the hippocampus and cortex, with the interactions of three oscillations representing memory trace reactivation and transmission (Born & Wilhelm, 2012; Rasch & Born, 2013). The hippocampus acts as temporary storage, while the cortex functions as long-term storage, and the thalamus serves as a relay for information transmission (Klinzing et al., 2019). In the hippocampus, reactivation events occur during ripples nested within spindles, which induce synaptic plasticity in learning-related circuits (Fernandez & Lüthi, 2020). A subset of these spindle-ripple events is enveloped within the excitable rising phase (UP state) of global SOs, which serve as a pacemaker for information transfer between the hippocampus and neocortex (Niknazar, Malerba, & Mednick, 2022). This framework is supported by evidence in both rodents and humans, which will be introduced in detail in the following two sections.

Animal Evidence. In rodents, a large body of evidence demonstrates that SWRs characterize memory reactivation. The incidence of SWRs increases after learning and discontinuing them interferes with memory consolidation (Davidson, Kloosterman, & Wilson, 2009; J. Patel, Schomburg, Berényi, Fujisawa, & Buzsáki, 2013). More convincing evidence comes from the sequence replay of hippocampal neurons during sleep, where neurons (considered part of the memory engram) that fire in a specific temporal order during a behavioral task will re-fire in the same sequence during subsequent NREM sleep, typically associated with SWRs. However, although the sequence of firing is identical to that during wakefulness, the duration of such a sequence completion is shorter during sleep (Fig 1.6; Clawson et al., 2021; Diba & Buzsáki, 2007; Euston, Tatsuno, & McNaughton, 2007; Lansink et al., 2008; A. K. Lee & Wilson, 2002; O'Neill, Pleydell-Bouverie, Dupret, & Csicsvari, 2010).

Sleep spindles are associated with rhythmic, synchronized neuronal activity between pre- and postsynaptic neurons and can trigger long-lasting synaptic plasticity changes via activation of Ca^{2+}-

dependent signaling pathways (Lüthi & McCormick, 1999; Fernandez & Lüthi, 2020)**.**

The modulation of related oscillations by slow waves has also been demonstrated. During the DOWN-UP transition of SOs, the synchronous firing of new cortical neurons may be a timing trigger for SWRs (Isomura et al., 2006). Applying slow oscillatory electrical stimulation to cortical areas of cats and macaque monkeys induced spindle-like self-sustained oscillations, demonstrating that the depolarization phase of SOs may drive thalamic spindle generation (Steriade, 2006). Studies in rodents suggest that the accuracy of memory reactivation and consolidation behavior is associated with the precision of coupling between SOs and spindle activity (Silversmith et al., 2020). Plasticity conditions, such as activity in Ca^{2+} pyramidal neurons, are enhanced when spindles are nested within SOs (Niethard, Ngo, Ehrlich, & Born, 2018)

Figure 0.6. Replay of Neuronal Spike Sequences During Sleep

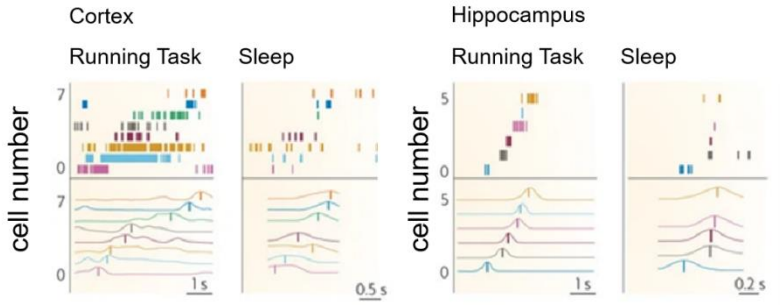

Note. Smoothed place fields (colored lines) of eight place cells during runs from left to right on a track (average of 30 trials). Vertical bars mark the positions of the normalized peaks of the smoothed fields. The non-uniform time axis below shows time within an average lap when the above positions were passed. Bottom panels: three SWRs - related sequences from SWS after the waking session. The sequences during SWRs and run were similar but different in timescale (the white bar on the upper-left corner stands for 50ms). Figure from A. K. Lee & Wilson, 2002.

Human Evidence. Intracranial EEG (iEEG) studies have shown that during slow oscillations (SO), neuronal firing rates increase during the UP state and decrease during the DOWN state across the entire brain (Nir et al., 2011). Brain-wide coherence increased during the SOs UP state after a declarative

learning task (Mölle, Marshall, Gais, & Born, 2004). Some studies have quantitatively analyzed the relationship between SWS and memory retention, such as the positive correlation between the SWS amount and the performance of declarative memory (Holz et al., 2012), and decreased SWS in older adults is associated with degeneration of the prefrontal cortex, affecting declarative memory performance(Ba et al., 2013). Moreover, the benefits of sleep for memory are optimized when spindles consistently couple with SOs peaks (Hahn, Bothe, et al., n.d.; Hahn, Heib, Schabus, Hoedlmoser, & Helfrich, n.d.; Halonen, Kuula, Antila, & Pesonen, 2021; Helfrich, Mander, Jagust, Knight, & Walker, 2018)**.**

Some studies explore the impact of oscillatory coupling on memory performance by artificially applying external oscillations, thereby indirectly reflecting reactivation phenomena. For instance, artificial interventions such as closed-loop, in-phase auditory stimulation (Ngo, Martinetz, Born, & Mölle, 2013), slow oscillatory transcranial direct current stimulation(Westerberg et al., 2015; Paßmann et al., 2016), and pharmacological interventions like interleukin-6 (Benedict, Scheller, Rose-John, Born, & Marshall, 2009) and sodium oxybate (Hall, 2009) can enhance low-wave power and/or SWS duration in human subjects. These interventions lead to increased slow-wave-related metrics, further improving the consolidation of declarative memories during sleep.

Due to ethical and technical constraints, there is difficulty in observing SWRs signals in deep brain regions in general noninvasive EEG studies. Researchers face a significant challenge in pinpointing memory reactivation. Targeted Memory Reactivation (TMR) is one approach to address this issue. With TMR, cues such as odors or sounds associated with newly learned material are presented to individuals during sleep to reactivate specific memories. Studies have found that TMR stimulation during SWS can enhance visual-spatial memory (Hu, Cheng, Chiu, & Paller, 2020; Rudoy, Voss, Westerberg, & Paller, 2009). TMR cues lead to a significant increase in sleep spindle activity, and retention was enhanced by cues and predicted by post-cue spindles (Antony et al., 2018; Laventure et al., 2018). This evidence

indicates that TMR evokes neural oscillatory activity patterns associated with memory reactivation and consolidation.

In addition, there are also studies investigating reactivation from a neuroimaging perspective. Many fMRI studies repeatedly demonstrate that brain regions involved in learning re-engage during subsequent sleep, and the level of re-engagement correlates with the behavioral benefits of memory consolidation during sleep (Bergmann, Mölle, Diedrichs, Born, & Siebner, 2012; Boutin et al., 2018; Fogel et al., 2017; Peigneux et al., 2004). For example, in a face-location memory experiment, functional connectivity between the whole brain and the fusiform face area (FFA) was separately calculated during learning and sleep states. It was found that the regions showing significant connectivity with the FFA during sleep overlapped with those during learning (Van Dongen et al., 2011).

In summary, studies have provided valuable insights into the memory consolidation processes during human sleep, particularly concerning the interactions between SO and spindle wave activity in SWS, their associations with memory performance and memory cues, as well as the activation of relevant memory brain regions. However, evidence that more directly reflects memory reactivation is still limited.

MVPA in Memory Reactivation Study

MVPA is a brain imaging method, particularly used with fMRI, that decodes cognitive processes by analyzing spatial patterns of brain activation (Peelen & Downing, 2023). Unlike traditional univariate activation studies, MVPA delves into how voxels within each region of interest (ROI) respond to different stimuli. Voxels in an fMRI scan partly reflect neural activity around them, and each voxel within an ROI may respond differently to various stimuli. By combining responses from multiple voxels, unique response patterns specific to a stimulus can be obtained, which remain similar across multiple scans. This means that instead of studying isolated numbers, MVPA provides multidimensional numerical vectors representing responses evoked under specific conditions, with each dimension representing a

voxel (Kubilius, Baeck, Wagemans, & Op de Beeck, 2015). By computing the correlation between these vectors, differences and similarities between conditions can be revealed (Haxby et al., 2001; Misaki, Kim, Bandettini, & Kriegeskorte, 2010). If response patterns were similar between two conditions, their correlation would be high; conversely, if response patterns differ, the correlation would be low. MVPA methods offer a way to decode the content of memory to some extent, providing direct evidence of memory reactivation(Polyn, Natu, Cohen, & Norman, 2005).

In addition to correlation analysis, machine learning methods can be used to identify overall brain patterns. Machine learning is a technique that allows computers to learn patterns from data and then use these learned patterns to make predictions or decisions (Murphy, 2012). At present, many machine learning methods have been applied in MVPA, such as linear support vector machines (SVM; Kamitani & Tong, 2005; Mitchell et al., 2004), linear discriminant analysis (LDA; Haynes & Rees, 2005a, 2005b) and neural networks (Polyn et al., 2005). The basic principle of using machine learning in MVPA is to consider the neural activity intensity of each voxel as a feature (Logothetis & Wandell, 2004). Each multidimensional numeric vector obtained from activations in each event serves as a training sample, with each activation pattern as a label (Norman, Polyn, Detre, & Haxby, 2006). By inputting data into an appropriate classifier, and after training and learning, weights are assigned to each feature to summarize the comprehensive activation patterns of each voxel under various conditions.

The application of the MVPA method in sleep and memory research provides a new perspective for understanding the neural mechanisms involved in memory consolidation. First, this method does not rely on external stimuli and can reveal spontaneous brain reactivation patterns during sleep, helping us better understand how memories are processed and strengthened in a spontaneous state (Denis & Cairney, 2023). Second, data extracted from fMRI voxels typically have high dimensionality, and using machine learning methods and corresponding dimensionality reduction method offers better adaptability in high-dimensional spaces (Kriegeskorte et al., 2006; Pereira et al., 2009). Third, MVPA is

beneficial for understanding the neural mechanisms underlying the processing of memory across the entire brain, as well as the coordination and interactions between different brain areas (Pereira, Mitchell, & Botvinick, 2009; Saeys, Inza, & Larrañaga, 2007).

At present, studies have applied the MVPA method in sleep memory reactivation. For example, one study used fMRI pattern analysis to track item-level replay in the hippocampus during an awake rest period after participants studied 15 objects and completed a memory test. Objects that were remembered less well were replayed more during the subsequent rest period, suggesting a prioritization process in which weaker memories—memories most vulnerable to forgetting—are selected for replay (Schapiro, McDevitt, Rogers, Mednick, & Norman, 2018). Another study tested whether neural representations of rewarded (compared to non-rewarded) events have priority for reactivation during sleep. They showed that patterns of brain activity observed during waking behavior spontaneously reemerge during SWS (Sterpenich et al., 2021).

However, one unresolved issue in the above studies is that memory reactivation during sleep occurs relatively rarely, with most brain states likely unrelated to memory processes. The studies referenced above primarily investigated different types of memory replay based on artificial labels (e.g., the vulnerability of memory, whether a reward was involved during memory encoding), while not comparing the memory reactivation state and other non-memory states during sleep. In other words, these studies can only predict the priority of memory type, but they cannot determine whether the current state is more characteristic of the memory itself than the normal sleep state without memory reactivation. Thus, the source and definition of memory reactivation and other sleep patterns require further exploration and experimentation.

Objectives and Hypotheses

Gap

The ASC framework has received strong evidence from animal studies, indicating that the

reactivation of hippocampal and cortical areas during SWS supports memory consolidation. While human studies support the correlation between SWS and memory consolidation, direct evidence of memory trace reactivation during SWS in humans remains limited due to technical and ethical constraints.

Objective

This study focuses on brain imaging activation patterns related to visual-spatial memory. We utilize the MVPA method to identify memory reactivation during sleep, aiming to explore the characteristics of memory reactivation across different sleep stages and thereby provide direct evidence for the active system consolidation framework.

Hypotheses

We hypothesize that brain patterns resembling memory recognition during wakefulness preferentially reactivate during SWS compared to other sleep stages

Material & Method

Experiment

The study protocol was approved both by the Research Ethics Committee of the University of Electronic Science and Technology of China and McGill University. We complied with all relevant ethical regulations for work with human subjects. All participants gave their written informed consent to take part in this study and received financial compensation for their participation. The author affirms that the human research participant provided informed consent for the publication of the photographs in Fig. 2.4 and Fig. 2.6.

Overall Process of Experiment

The overall process of the experiment is shown in Fig 2.1. The main experiment lasted from the evening of the first day to the morning of the second day and includes three parts: **Pre-sleep, Sleep, and Post-sleep**. Here, we recorded participants' fMRI data while they were doing several types of visual-spatial memory tasks before and after sleep (see the part of task paradigm) and simultaneous fMRI-EEG data in subsequent sleep.

Pre-sleep. Participants arrived at 21:00 after showering. After a short training, the Pre-sleep part started at around 21:30. Subjects were scanned while doing an object-location memory task, including the two blocks of the Encoding Task and four blocks of the Retrieval Task. This part finished at 22:10, then participants were equipped with an MRI-compatible EEG device, and they were free to take a break and go to the washroom until 23:00.

Sleep. The Sleep part included a 100-minute scan synchronized with EEG collection. Before the scan began, the subjects were adjusted to a comfortable position, and padding was placed around the head to cushion and prevent head motion. After the scan, participants were awakened and went to another room to continue sleep until the second morning.

Post-sleep. On the second day at 8:00 participants were awakened and escorted to wash their

faces, brush their teeth, and shampoo their hair. The Post-sleep part began at 9:00. In this session, delay memory was tested, including four blocks of the old-new recognition task and two blocks of delay object-location retrieval task.

Figure 0.1. Experimental Overview

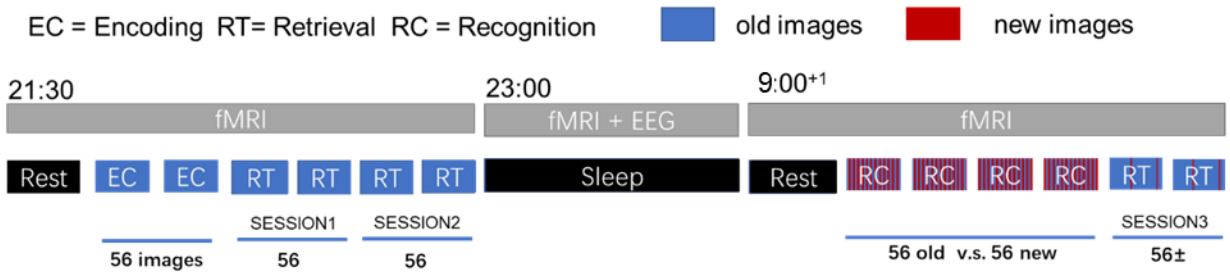

Note. EC denotes the object-location memory **Encoding** process, RT denotes the object-location memory **Retrieval** process, and RC denotes the old-new memory **Recognition** process. The black boxes represent task-free resting or sleep scans, the blue ones represent the stimuli presented as old pictures, the red ones represent new pictures, and the alternating red and blue stripes represent the alternation of old and new pictures.

To enhance the likelihood of participants falling asleep during the experiment, we instructed them to postpone their bedtime by one hour the night before the experiment and to wake up at their usual time on the morning of the experiment day, following the protocol of a previous study (Deuker et al., 2013). Participants were instructed to abstain from consuming caffeine, drugs, and tobacco, as well as from napping on the day of the experiment which was confirmed using scales administered on the day of the experiment.

Participant

This study initially recruited 11 healthy, right-handed participants through campus advertisements and online posters. However, due to participant dropout and incomplete sleep structure observed in EEG recordings, data from only 7 participants (4 women, 3 men; mean age ± SD: 21.00 ± 1.85 years) were retained for analysis (Table 2.1). Each participant received 400 RMB as compensation upon completing the entire experiment.

All data were collected at the Magnetic Resonance Imaging (MRI) Center of the Qingshuihe Campus, University of Electronic Science and Technology of China. Prior to the experiment, all participants underwent interviews via phone calls and online surveys to confirm their eligibility. Exclusion criteria included neurological, psychiatric, or sleep disorders; color vision abnormalities; metal implants; and claustrophobia. Additionally, questionnaires were administered to assess participants' sleep quality and mental health status (Table 2.1).

Table 0.1. Information for Analyzed Samples, including Gender, Age, and Questionnaire Results

	Gender	Age	ESS	BDI	PSQI	MEQ
Sub1	M	24	5	0	2	52
Sub3	F	22	7	1	1	49
Sub4	M	19	9	2	2	60
Sub5	F	20	9	0	1	59
Sub6	F	19	5	1	1	47
Sub7	M	20	4	1	1	58
Sub9	F	23	6	2	2	46
MEAN	/	21.00	6.43	1.00	1.43	53.00
SD	/	1.85	1.84	0.76	0.49	5.50
Reference	/	/	0~10	0-13	0-4	/

Note. Questionnaires including ESS = Epworth Sleepiness Scale, BDI = Beck Depression Inventory, PSQI = Pittsburgh Sleep Quality Index, MEQ = Morningness-Eveningness Questionnaire (comprising 5 types: Definitely Evening Type (16-30), Moderately Evening Type (31-41), Neither Type (42-58), Moderately Morning Type (59-69), Definitely Morning Type (70-86)). Participants exhibited no abnormal sleepiness symptoms, no signs of depression, no extreme sleep schedules, and reported good sleep quality.

Task Paradigms

A total of 56 pairs of high-definition colorful pictures of real objects were selected from the library of the Department of Psychology, University of California, San Diego. Each of these pairs was broadly similar, with only minor differences (Fig 2.2 c).

The experiment included two types of memory tasks. One was to recognize the old and new item memory, corresponding to the old-new recognition task. The other was the context memory to memorize the item and location association information, corresponding to the object-location retrieval

task. Additionally, since there were three sessions of the object-location retrieval task (two immediately after encoding and one on the second day), for ease of comparison, these three blocks are named Session1, Session2, and Session3.

Encoding Task (Fig. 2.2 a). During each trial, subjects passively watched 56 pictures (one picture in each pair) and memorized their corresponding positions marked by the green circle located on one of the four corners of the screen within 3 seconds. Then the picture moved to its corresponding position and remained fixed for 2 seconds. This task included a total of 56 trials.

Object-location Retrieval Task (Immediate) (Fig. 2.2 b). There were two circles of retrieval tasks immediately after the encoding. The 56 pictures in the last task were randomly displayed in each trial of the first circle in two blocks and repeated in the second circle. In each trial, subjects responded to the picture shown on the screen and chose one of the four positions using a remote keypad according to the encoded memory within 3s. If the response was correct, the circle on the corresponding location turned from gray to green; if incorrect, the color of the chosen position turned red. After that, the picture moved to the correct position and remained there for 2s. This task included a total of 112 trials.

Old-new Recognition Task (Fig. 2.2 c). 112 pictures were displayed randomly in this task on the second day. In addition to the 56 pictures encoded and retrieved last night (old group), the other half of the 56 pairs were also added (new group). In each trial, subjects would respond within 3 s by pressing the keyboard to indicate if the picture was old or new. The left button indicates new while the right one means old. After the response, the corresponding circle on the screen turned black. There was no feedback on this task. This task included a total of 112 trials.

According to the true type of the picture and the subject's choice, there were four types of outcomes for the old-new recognition task, including **HIT** (old pictures identified as old), **MISS** (old pictures identified as new), **CORRECT REJECTION** (new pictures be chosen as new) and **FALSE ALARM** (new pictures identified as old).

Object-location Retrieval Task (Delay) (Fig. 2.2 d). The program would record and select the pictures that were chosen as 'old' in the recognition task and display them in this task. If the subject considered the picture to be old, they would select the right circle; otherwise, they would select the left circle. The process was the same as the immediate retrieval task, only without any feedback. This task included approximately half of the previous task (depending on the number of old pictures chosen in the last task, MEAN=54.57, SD=6.37).

Figure 0.2. Flowchart of the Four Memory Tasks

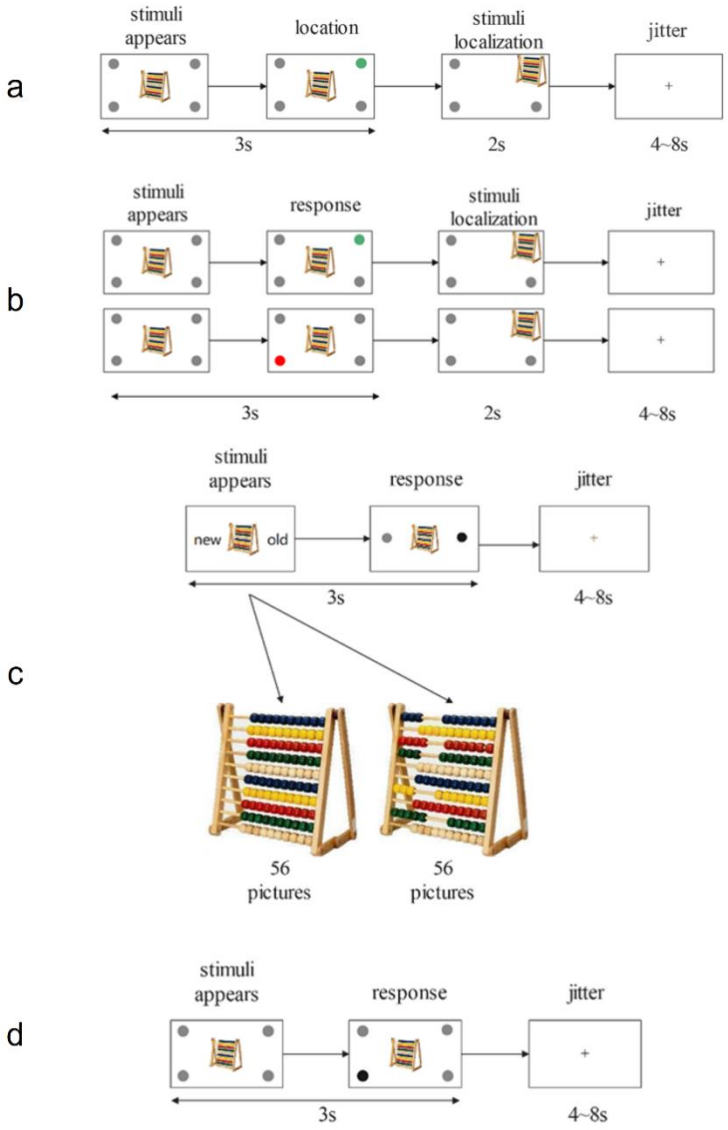

Data Acquisition

fMRI. The fMRI data was recorded on a 3T MRI scanner (GE DISCOVERY 750) using a 12-channel head coil. The structural images were acquired using T1-weighted imaging sequences, while all fMRI images were collected using echo planar imaging (EPI) sequences. EPI acquisition parameters are as follows: 42 axial slices, repetition time (TR) =2000ms, no layer interval, echo time (TE) =30ms, layer thickness =3mm, field of view (FOV) =192×192mm^2, image matrix size 64×64, voxel size 3×3×3mm^3. T1

scanning parameters are as follows: 152 axial slices, repetitions time (TR) = 5.972ms, no layer interval, echo time (TE) =1.968ms, layer thickness =1mm, field of view (FOV) =256×256mm^2, image matrix size 256×256, voxel size 1×1×1mm^3.

EEG. EEG data were collected using an MR-compatible EEG cap (64-channel, Neuroscan, SynAmps, RT) with electrodes placed following international 10-10 system standards, together with 2 ECG electrodes placed 1cm above and below the corners of the eyes on both sides, and 2 EOG electrodes placed on the left rib and right clavicle. The electrode resistance was reduced to less than 10kΩ before the collection. The sampling rate was set as 5000Hz during recoding.

Preprocessing

fMRI. First, the original format exported by the MRI scanner was two-dimensional DICOM format, and all data were converted to three-dimensional NifTi format using SPM, facilitating subsequent computation and analysis.

Due to the spatial stretching affine transformation, interpolation, and smoothing processes involved in coregistration, there may be signal loss and distortion. Additionally, given the small number of participants and the considerable differences in activation patterns between individuals, focusing solely on group-level activation areas may not effectively predict sleep reactivation. Therefore, after the steps of time slicing and realignment, the process of coregistration was done in individual spaces. This approach helps reduce information loss in sleep fMRI data and enhances the model's sensitivity to individual memory reactivation patterns. The individualized coregistration specifically targeted the following two data components:

1) Sleep structural imaging data: The sleep structural imaging data of each individual determined the basic coordinate system for model training. The T1 structural images scanned before the sleep stage were down-sampled to a resolution of 2×2×2mm^3 using DPABI (Yan, Wang, Zuo, & Zang, 2016) software. This step adjusts the voxel size to an appropriate granularity, improving the efficiency of

model training and reducing the interference of random noise in subsequent steps. The bet command from FSL (McCarthy, 2024) was used to remove the skull from the structural images, with the threshold parameter set to 0.5. Skull stripping facilitates the alignment of masks to individual spaces in later steps.

2) Old-new item memory functional imaging data: After the images underwent time slicing and realignment, the parameters for spatial coregistration were modified to align the functional images with the structural images obtained in the previous step before removing the skull.

In addition, because this study was conducted in the subject's individual space, there was no need for group-level analysis; combined with the impact on the data quality, normalization and smoothing steps were omitted in the pre-processing process.

EEG. EEG preprocessing was performed using Curry 7 software (Compumedics Neuroscan). First, gradient artifacts were corrected by subtracting a constant 15-point whole-brain sliding average. Then, a high-pass filter was applied at 0.1 Hz, a low-pass filter at 35 Hz, and the data were down-sampled to 250 Hz. Cardiac pulse artifacts were detected using a threshold method and corrected by subtracting the first three principal components (Qin, 2020). Finally, the preprocessed EEG data were staged according to the AASM Manual for the Scoring of Sleep and Associated Events (Berry et al., 2017).

Table 0.2. Statistics of Participants' Sleep Structure

Sleep Stage	Duration(min) (Mean±SD)	N
W	34.00 ± 14.71	10
N1	30.70 ± 18.72	10
N2	21.25± 14.88	8
N3	13.70 ± 13.15	7
REM	0.35 ± 0.78	2

Sleep staging was manually scored by experts from Chengdu Fifth People’s Hospital, according to AASM criteria (Iber et al., 2007). For the 100-minute sleep period, every 30s epoch was scored as W, N1, N2, N3, or REM sleep, and SWS was determined as the non-REM sleep stage 3 (N3). Table 2.2 shows the sleep structure of the participants and the number of individuals who entered each sleep stage.

Among all the participants, 1 exited the sleep session midway, and the remaining all entered the N1 sleep stage. Seven reached SWS and two reached REM sleep. Complete data from the seven participants were obtained for further analysis.

Model Training

In the previous chapter, the experimental paradigm design and overall process, as well as behavioral, fMRI, and EEG data acquisition, were introduced. To study the reactivation of memory during sleep, this chapter will employ the MVPA method and train a memory reactivation model for each subject based on the fMRI data from the memory task. The data during the old-new recognition task in different states were used as the training set to extract memory activation patterns under different sleep stages. MVPA training used Nilearn (Abraham et al., 2014) and scikit-learn toolbox (Pedregosa et al., 2011).

Process of Model Training

Dataset Definition. Three types of labels were defined in the dataset: HIT, CORRECT REJECTION, and REST. HIT and CORRECT REJECTION originate from behavioral classifications in two sequences of the new-old memory task, while the REST state comes from the wakefulness period before officially falling asleep during sleep scans (Table 2.3).

Table 0.3. Source, Meaning, and Function of Three State Labels in the Dataset

Label	Dataset Source	Physiological Meaning	Function in Model
HIT	Old-new Recognition Task	Memory Reactivation	Aim state
CORRECT REJECTION	Old-new Recognition Task	Novel Detection	Control
REST	W Stage before Falling Asleep	Close-eye Rest	Control

The HIT state indicates the correct recognition of old items, defined as a memory reactivation pattern, which this study aims to identify during sleep. CORRECT REJECTION denotes the correct detection of new items. Since new items only appear in the experiment on the second day, any patterns

like CORRECT REJECTION during sleep cannot be memory reactivation patterns, thus considered a control state. This concept stems from Deuker et al.'s (2013) study, which used post-sleep task states as a control for sleep memory reactivation, achieving good results. REST data come from the first 10-50 whole-brain fMRI scans during the sleep stage. EEG staging data shows that these images were all scanned when the subjects were in the W stage. The REST pattern represents a wakeful rest stage which is another control state.

For each HIT and CORRECT REJECTION state training sample, the most representative scanning volume from each memory task sequence was extracted. In the experiment, each participant performed four sets of old-new recognition tasks, with each set containing 28 sequences.

Figure 0.3. Diagram of One Trial and the Aim TR inside

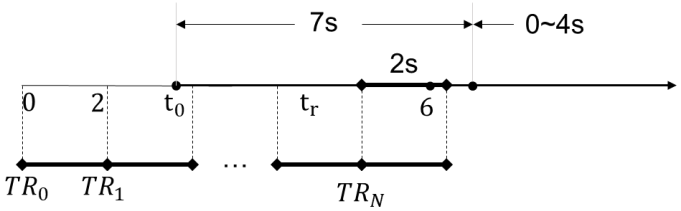

Note. The arrow in the middle of the figure represents fMRI scan sequences onset from 0s, with each scan TR occurring every 2 seconds and labeled sequentially as TR_0, TR_1, etc. Here, TR_N refers to the specific N^{th} TR selected as a sample within the trial starting at t_0. The selection for TR_N should meet two rules: 1) TR_N is contained within the trial starting at t_0, and 2) TRN occurs approximately 5-6 seconds after the trial onset.

According to a previous study (Connolly et al., 2012), the volume approximated to the 5th - 6th second after the stimuli onset (the time-to-peak of the HRF curve) and within the trial would be picked as one sample in each trial. Because one trial in the recognition task was jittered around 7s - 11s and the TR of scanning was 2s, which TR to pick in each trial was not fixed.

The method to pick up one volume in each trial is as follows where "⌊⌋" means round down:

$$N = \lfloor (t_o + 5)/2 \rfloor = 2 + \lfloor (t_o + 1)/2 \rfloor$$

The start time of the scanning sequence calculated using this method falls between 3-5 seconds,

and the end time falls between 5-7 seconds, ensuring that the selected scanning sequence represents the maximum activation during the trial (Fig. 2.3).

Mask Selection

As a step of feature selection, a mask was selected for each subject to filter and get the most effective 500 voxels from the whole brain to act as features of the dataset (Fig. 2.4).

Figure 0.4. Pipeline to Train the Mask

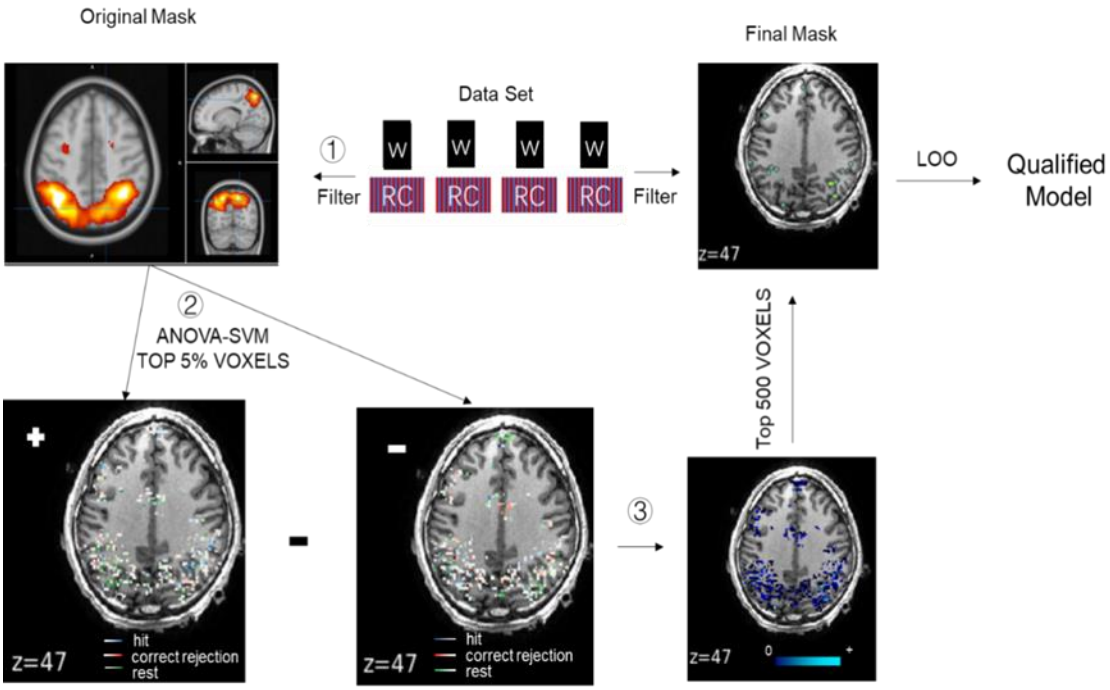

Note. In the dataset, W represents 40 whole brains representing REST samples extracted during the waking period of sleep, and RC represents two types of samples representing HIT and CORRECT REJECTION extracted during the new and old recognition tasks. Mask training was divided into three steps, and the final mask was used to extract the 500 voxels that can best distinguish the three states from the original feature data for classifier training of the reactivated model.

First, each sample from the dataset was filtered by an original mask. The mask was provided by the website NeuroQuery under the index “Memory Retrieval” and was a predicted distribution of activations summarized from the literature (Dockès et al., 2020). The original mask was coregistered to

the reference cranial removed structural image scanned before the sleep session by FSL (McCarthy, 2024). Second, the filtered samples were marked by the three task-related labels, and the ANOVA-SVM method in the Nilearn toolbox was used to find the top 5% activated voxels in the three types of tasks. Weight coefficients, indicative of activation levels, were assigned to each selected voxel. Positive coefficients add the likelihood of activation during the corresponding task, while negative coefficients reduce the likelihood, aiding in distinguishing between task types. Third, the positive and negative part of the weight coefficient map in each label was separated into six components, and the negative maps were subtracted from the positive maps, yielding a comprehensive map representing the sum of the absolute values of all six components. A higher value in this map indicated greater predictive power across all three conditions. Finally, the top 500 voxels from this overall map were selected to generate the final mask, which were the 500 points with the highest predictive power for the three states.

Classifier

Support Vector Machine (SVM) classifier was used with the LinearSVM function from the Scikit-learn toolbox. The fundamental principle of SVM involves finding a hyperplane that maximizes the margin between classes, ensuring effective sample classification. To address multiclass classification, the One-vs-Rest (OvR) strategy was employed, constructing individual hyperplanes each time to distinguish one type from the rest, and this process was repeated three times. For a given sample i with a feature vector $\boldsymbol{x}_i$ (of length 500) and the corresponding label y_i, the objective during each plane partition is to find a hyperplane $\boldsymbol{\omega}^T\boldsymbol{x}_i + b$, such that the following objective is satisfied:

$$\min_{\boldsymbol{\omega}} \frac{1}{2}\boldsymbol{\omega}^{\mathrm{T}}\boldsymbol{\omega} + \mathrm{C}\sum_{i=1}^{l}\xi(\boldsymbol{\omega}; \boldsymbol{x}_i; y_i)$$

$$\text{s.t. } y_i\left(\boldsymbol{\omega}^{\mathrm{T}}\boldsymbol{x}_i + b\right) \geq 1, \quad i = 1, \ldots, l$$

Where i is the number of features, and ξ is the loss function. Here the l_2 loss function was used:

$$\xi(\boldsymbol{\omega}; \boldsymbol{x}_i; y_i) = \max\left(1 - y_i\boldsymbol{\omega}^{\mathrm{T}}\boldsymbol{x}_i, 0\right)^2$$

After the completion of model training, three hyperplanes were obtained, represented by three

sets of parameters ($\boldsymbol{\omega}$ and corresponding b values). The hyperplane with the maximum margin corresponds to the category of the sample. LLet'sj denote the sample label category, and the decision function is as follows:

$$f(\boldsymbol{x}_i) = \text{argmax}_{j\in\{1,2,3\}}[(\boldsymbol{\omega}^j)^{\mathrm{T}}\boldsymbol{x}_i + b^j]$$

After the model was trained, each input sample (whole-brain fMRI) was extracted through a mask to obtain 500 voxels as features. Then, the model could calculate the likelihood of the sample being in one of the three target states, and the sum of the three likelihoods is 1.

Model Verification

Sample Balance. Table 2.4 shows the number of three types of samples for each subject in the model training set. In the old-new recognition task, each participant performed four blocks of tasks, each containing 28 sequences for a total of 112 sequences. The average ratios of HIT and CORRECT REJECTION in all sequences were close, and the number fluctuated around 40. The REST sample was taken directly from the 10th to 50th TR of the sleep scan, and the sample number was fixed at 40. Therefore, the quantity of the three types of samples was balanced, and there was no excessive preference for a certain category, suitable for model training and verification.

Table 0.4. Sample Size of the Three Categories in the Dataset

	Sample Size		
No.	HIT	CORRECT REJECTION	REST
Sub1	36	42	40
Sub3	54	54	40
Sub4	48	46	40
Sub5	48	36	40
Sub6	52	49	40
Sub7	53	47	40
Sub9	41	51	40
Mean	47	46	40

Cross-validation Results. To test the model's performance, each subject's sample was divided into four groups based on the grouping in the experiment, and then the 40 REST state whole-brain

samples were also divided into four groups to be combined with the experimental groups. Thus, the final training set consisted of 4 groups, each containing about 30 samples (including about 10 HIT about 10 CORRECT REJECTION, and 10 REST), with balanced quantities for each label. Cross-validation was performed using the leave-one-out method, with data from 3 groups used for training and 1 group for testing each time. The same group division method was adopted during validation to ensure consistency between the training and validation sets, better simulating real conditions and obtaining a more realistic model performance.

Table 0.5. Average Accuracy in the Cross-validation of Each Subject's Model

	Accuracy			
No.	HIT	CORRECT REJECTION	Rest	Mean
Sub1	100.00%	100.00%	100.00%	100.00%
Sub3	96.30%	100.00%	97.50%	97.97%
Sub4	91.67%	73.91%	100.00%	88.06%
Sub5	87.50%	91.67%	100.00%	92.74%
Sub6	76.92%	97.96%	100.00%	90.78%
Sub7	83.02%	82.98%	100.00%	87.86%
Sub9	78.05%	94.12%	100.00%	90.91%
Mean	87.64%	91.52%	99.64%	92.53%

Figure 0.5 ROC Curve for the Model

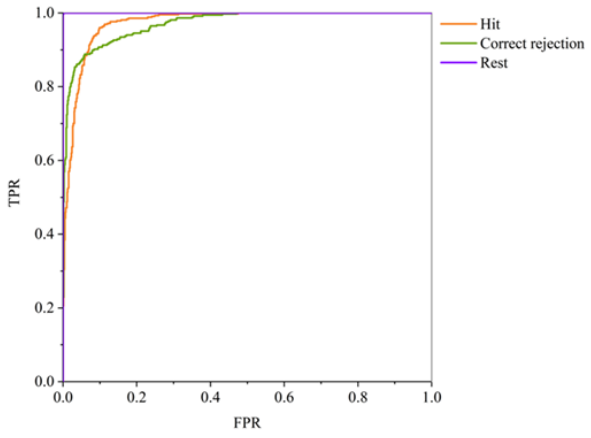

To evaluate the model's performance, leave-one-out cross-validation was employed. In each iteration, three blocks of data were used for validation, and one block was used for testing. Table 2.5

presents the average accuracy for each participant. The average accuracy for HIT, CORRECT REJECTION, and REST in the cross-validation was 87.64%, 91.52%, and 99.64%, respectively. The overall average accuracy for the three categories across all participants was 92.53%.

Another evaluation metric for the model is the Area Under the Curve (AUC). The ROC (Receiver Operating Characteristic) curve is a graphical analysis tool used to describe the relationship between the True Positive Rate (TPR) and the False Positive Rate (FPR) at different thresholds for a classifier (Fig 2.5). The horizontal axis represents the FPR, and the vertical axis represents the TPR. This curve reflects how the performance of the classifier changes with the variation in the classifier threshold. The AUC is the area under the ROC curve, with values ranging from 0.5 to 1. The closer the AUC is to 1, the better the performance of the classifier; conversely, the closer it is to 0, the worse the performance. The AUC value reflects the overall performance of the model at different thresholds and can indicate the model's stability.

This study analyzed the average AUC performance of three types of samples for all subjects. The results showed that the average AUCs for HIT, CORRECT REJECTION, and REST were 0.971, 0.973, and 1.000, respectively, with relatively smooth ROC curves (Fig. 2.5). This indicates that the model can maintain good performance across different decision thresholds, demonstrating high robustness and reliability.

Function of Hippocampus in State Prediction. The previous discussion demonstrated that the final trained mask comprises the 500 points with the highest predictive power for the brain. According to the active consolidation theory, the hippocampus should be involved in the reactivation process of target memory and thus should also play a role in the final model. To test this hypothesis, I counted the number of voxels in the final mask within the hippocampal region for each subject (as shown in Fig. 3.4). The results (Table 2.6) indicate that 6 out of 7 subjects exhibited activation in the hippocampus. Among these subjects, two (sub1 and sub7) had a higher proportion of hippocampal voxels in the final mask

compared to the original mask. These findings suggest that the hippocampus played a role in state classification for most subjects. However, in many subjects, the hippocampus did not show higher predictive power, implying that the final state classification likely relies on the joint involvement of multiple brain regions.

On the other hand, I retrained the model using the hippocampus as the original mask, selecting 500 voxels as the final mask using the same procedure, and then performed cross-validation (Fig 2.6). The results are shown in Table 2.7. The average cross-validation accuracy across all participants was 74.34%. While this is a decent average, the prediction results for HIT or CORRECT REJECTION were less than ideal for some participants. This result further supports that the hippocampus is involved in the target memory process and has some predictive power for state classification. However, for higher accuracy, it is best to include a broader range of memory-related brain regions for comprehensive analysis.

Figure 0.6. Example of Final Mask Distribution in the Hippocampus

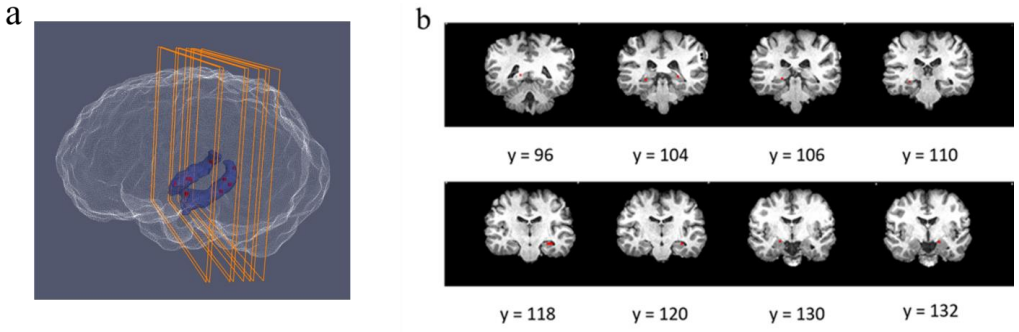

Note. Fig. a presents a glass brain illustration of the overlap between the individual spatial final mask of Subject 1 and the hippocampus. The blue areas represent the hippocampus, with each red box indicating a voxel in the final mask. The orange box marks the coronal slice taken through the voxel points in the final mask. The slicing results are shown in Fig. b, where each red square represents a voxel point in the final mask. The y-axis coordinates count from back to front with the unit of voxels, starting from the first slice of voxel as the coordinate y=1.

Table 0.6. Voxels and Voxel Proportion in the Final Mask for the Hippocampus and the Original Template

Across All Participants

No.	Final Mask Voxels in HPC	HPC Voxels	Final Mask Ratio in HPC	Final Mask Voxels	Original Mask Voxels	Final Mask Ratio in Original Mask
Sub1	11	1453	**0.76%**	500	111458	**0.45%**
Sub3	5	1385	0.36%	500	99335	0.50%
Sub4	6	1563	0.38%	500	106750	0.47%
Sub5	4	1404	0.28%	500	111147	0.45%
Sub6	6	1807	0.33%	500	99786	0.50%
Sub7	9	1554	**0.58%**	500	105824	**0.47%**
Sub9	0	1245	0.00%	500	116935	0.43%

Note. "Final Mask Voxels in HPC" refers to the number of Final Mask points within the hippocampal region for each participant. "HPC voxels" refers to the total number of voxels in the hippocampus itself. "Final Mask Ratio in HPC" indicates the proportion of hippocampal voxels selected as part of the Final Mask. "Final Mask Voxels" are the 500 voxels chosen by the ANOVA-SVM method, and "Original Mask Voxels" are those from the NeuroQuery template.

Table 0.7. Cross-validation Results after Training the Model Using the Hippocampus as the Original Mask

	Accuracy			
No.	HIT	CORRECT REJECTION	REST	Mean
Sub1	77.78%	45.24%	100.00%	74.34%
Sub3	71.11%	85.71%	100.00%	85.61%
Sub4	62.50%	93.48%	100.00%	85.33%
Sub5	85.42%	80.56%	100.00%	88.66%
Sub6	63.46%	81.63%	100.00%	81.70%
Sub7	63.46%	81.63%	100.00%	81.70%
Sub9	75.61%	76.47%	100.00%	84.03%
Mean	77.78%	45.24%	100.00%	74.34%

Model Accuracy after Shuffling Dataset. To validate the interpretability of the model, this study shuffled the sample labels to create a meaningless control dataset. Subsequently, this artificial dataset was re-entered into the model training process, including mask training and classifier training. We repeated the above process and conducted 100 cross-validations (see Fig. 2.7). The results showed that the classification accuracy significantly decreased after shuffling the labels, with an average drop of 18.7%. This significant performance decline indicates that the model's learning ability was notably reduced after shuffling. This further demonstrates that the three types of data in the original dataset

have clear and independent boundaries, and the model indeed captured the features of each category during the training process.

Figure 0.7. Comparison of Cross-Validation Accuracy Between Shuffled Dataset and Real Dataset

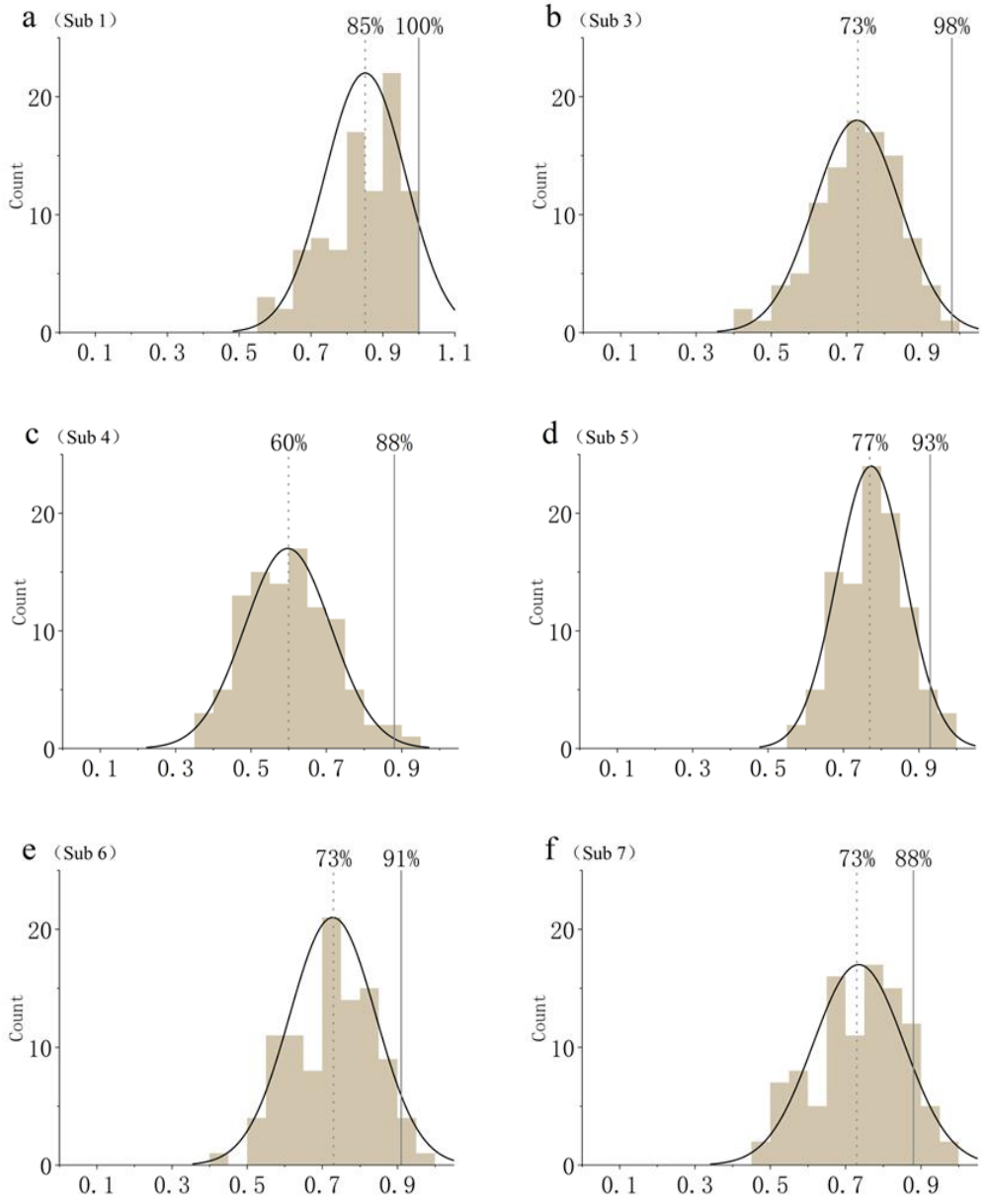

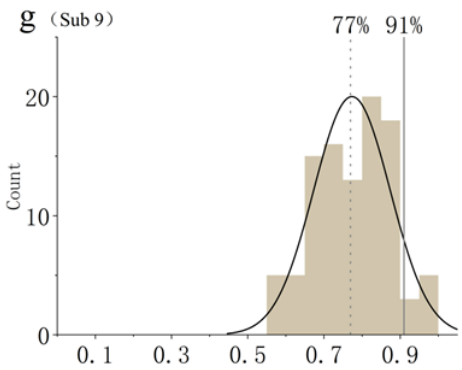

Note. The histogram in the figure represents the distribution of accuracy from 100 cross-validation iterations on a shuffled dataset, with the dashed line indicating the expected value of this distribution. The solid line represents the actual accuracy obtained from cross-validation on the original dataset. For all participants, the accuracy significantly decreases after shuffling.

Results

In the previous chapter, an MVPA model was trained for each participant, capable of predicting the likelihood of three states during sleep scans: HIT, CORRECT REJECTION, or REST. Here, HIT represents the target state of memory reactivation, CORRECT REJECTION and REST represents the control states.

To begin with, based on the previous assumptions, my expectations for the outcome were as follows: the REST state is considered an eyes-closed rest control state, which should show the highest likelihood throughout the scanning period. However, due to more complex activities occurring as participants entered asleep, the REST state was supposed more likely to be distributed in the W stages before actual sleep onset. CORRECT REJECTION was another control state, presented as a novel stimulus that was not shown to participants until the next morning, and its likelihood during the sleep scan period, whether in awake or sleep stages, should be low. The HIT state (target memory reactivation state) was expected to show a higher likelihood after entering sleep, especially during SWS periods.

This chapter will analyze participants' sleep data, exploring the correlation between sleep stages (W, N1, N2, and N3) and model predictions (HIT, CORRECT REJECTION, and REST) to further validate the hypothesis of this study that memory reactivation primarily occurs during slow-wave sleep. The analysis will begin with an overall examination of sleep stages and the three states. Following this, there will be a focus on the classification of memory states during N3 sleep. Finally, an analysis of behavioral data from memory tasks and their relationship with model-predicted brain states.

Global Analysis of Sleep

Effects of Subject

An analysis was conducted on the primary factors influencing participants' entry into the N3 sleep stage. Participants were grouped into those who eventually entered N3 sleep and those who did not. Statistical comparisons were made between the two groups based on gender ratio, age, and scale

results, with Mann-Whitney U tests conducted on continuous data other than gender (Table 3.1). The results indicated that the group entering the N3 stage had significantly higher scores on the ESS scale compared to the non-N3 group. The result suggested that a certain degree of sleepiness might facilitate deep sleep entry in this experiment.

Table 0.1. Statistics on Participants Entering and Not Entering the N3 Stage

Group	N3 (N=7)	Non-N3 (N=4)	Mann-Whitney U	p-value
Sex Ratio (M/F)	3/4	2/2	/	/
Age	21.00(1.85)	22.50(1.12)	7.50	0.230
ESS	6.43(1.84)	3.50(0.50)	27.00	**0.012***
BDI	1.00(0.76)	2.00(1.22)	8.00	0.315
PSQI	1.43(0.49)	1.00(0.71)	18.50	0.412
MEQ	53.00(5.50)	58.25(4.32)	5.00	0.109

Note. The first row in the table, Sex Ratio represents the ratio of males to females within each group, denoted as the number of males before the slash and the number of females after the slash. The second to sixth rows respectively show the mean and standard deviation (in parentheses) of age, Epworth Sleepiness Scale (ESS), Beck Depression Inventory (BDI), Pittsburgh Sleep Quality Index (PSQI), and Morningness - Eveningness Questionnaire (MEQ) scores for the two groups. Additionally, the table displays the Mann-Whitney U value and corresponding p-value for comparisons between the two groups, with '*' indicating a p-value less than 0.05.

Likelihood of Memory States in Different Sleep Stages

To estimate the likelihood of memory states in different sleep stages, the models were retrained using data from all four groups of the new-old recognition memory task as the train set, and the final trained model was applied to predict the states of sleep fMRI data. The function of CalibratedClassifierCV in scikit-learn was used for probability calibration. The function employed the Platt scaling algorithm (Platt, 2000) to estimate the likelihood assigned to each class sample, thus determining the probabilities of each brain reactivation state during the sleep process:

$$\mathrm{P}(y_i = j|\boldsymbol{x}_i) = \frac{1}{1 + \exp(\mathrm{A}f(\boldsymbol{x}_i) + \mathrm{B})}$$

Where j represents the sample label category, $\boldsymbol{x}_i$ represents the feature vector, and A and B are two parameters learned by the classifier. The model evaluated the likelihood of being in three states for

each sequence retained during sleep scans. Fig. 3.1 illustrates the likelihood of three states evaluated by the model during different EEG sleep stages for the 7 participants who eventually entered N3 sleep.

Figure 0.1. Memory Activation Across Different Sleep Stages

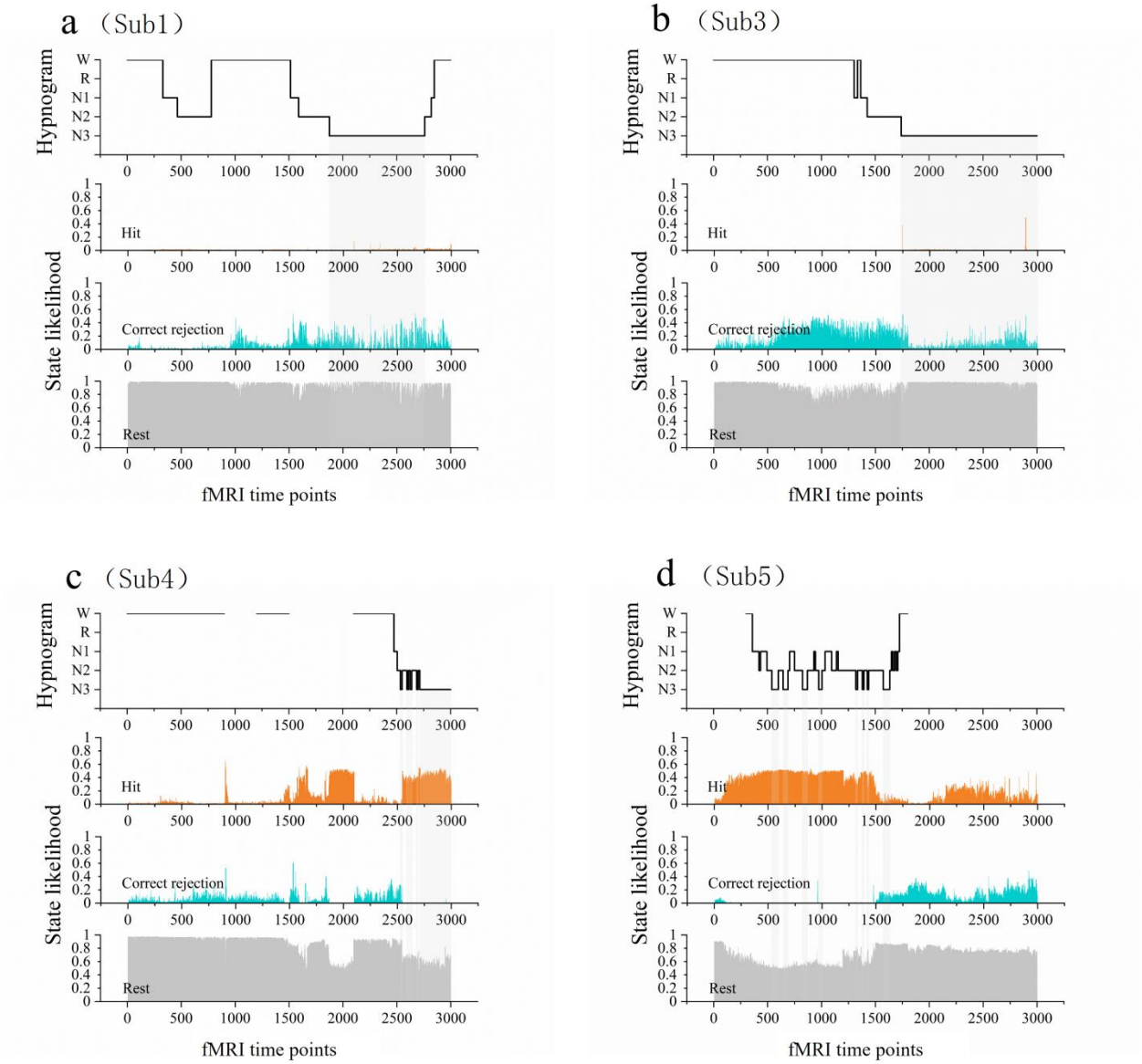

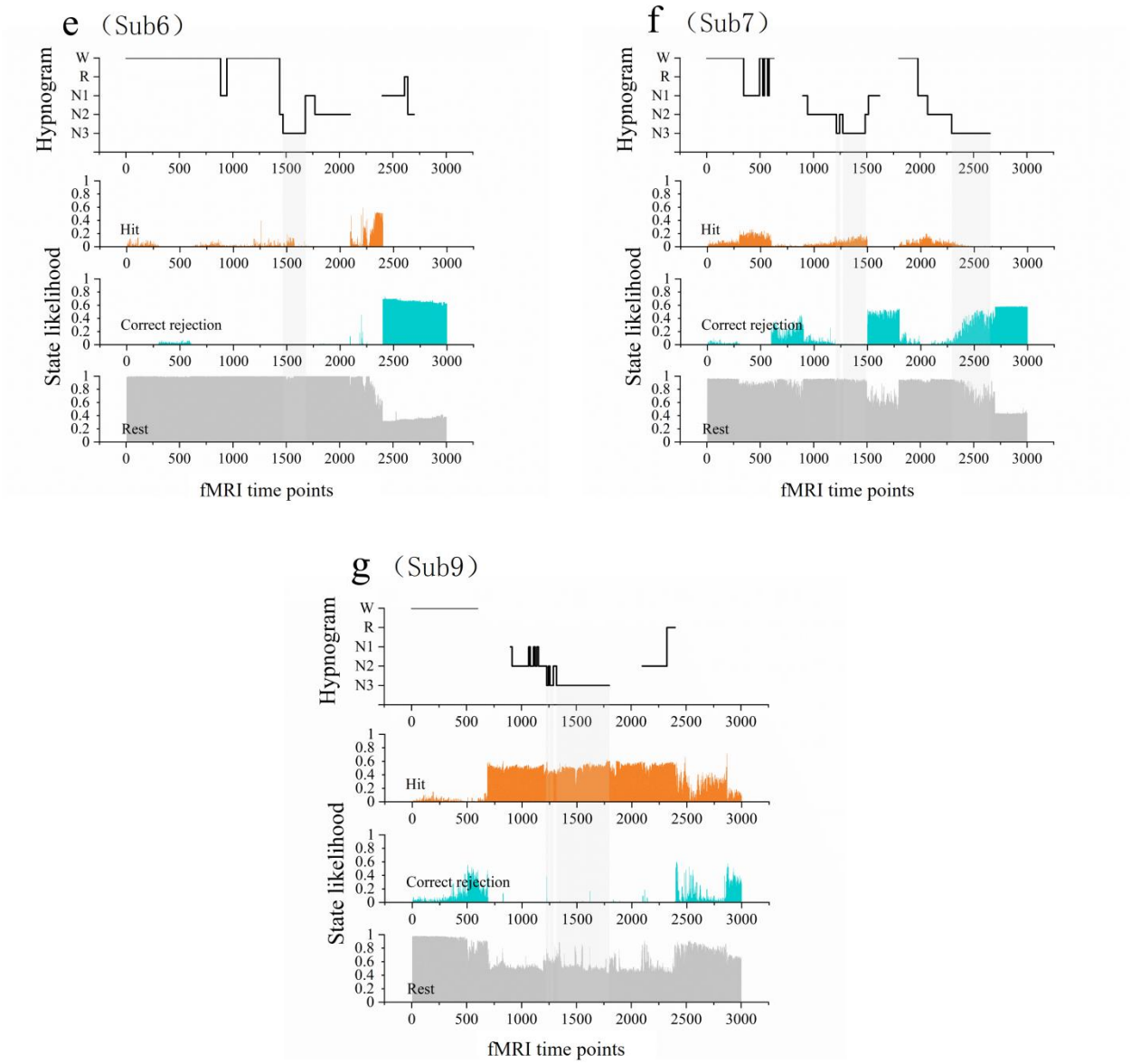

Note. In all figures, the x-axis represents 3000 time points throughout the entire sleep fMRI scanning sequence. The topmost step plot depicts the sleep cycles obtained from EEG staging across the entire scan period. Below are three histograms representing the likelihood of each TR being in one of three states. The orange histogram represents the HIT state, the blue histogram represents the CORRECT REJECTION state, and the gray histogram represents the REST state. Shaded areas in the figures highlight all time points corresponding to N3 stages.

From the figures, it can be observed that the overall activation likelihood of the REST state was highest across all participants, while activations in other states were more dispersed, which was consistent with the hypothesis. The distributions of the other two states appear more scattered, and

upon direct observation, they did not exhibit a specific pattern.

Furthermore, a comprehensive validation of brain states during wakefulness and sleep stages was conducted. Specifically, based on the determination of sleep onset from sleep staging, sleep stages were categorized into two classes: wake and other sleep stages (Fig. 3.2). The average likelihood of the three states was calculated for the two stages. For W state, the average likelihood of HIT state was 0.047, compared to 0.187 in other sleep stages; the average likelihood of CORRECT REJECTION state during wakefulness was 0.080, compared to 0.092 during sleep stages; and the average likelihood of REST state during wakefulness was 0.876, compared to 0.721 during sleep stages.

Figure 0.2. The Mean Likelihood for Seven Participants of the Three States during Wake and Other Stages

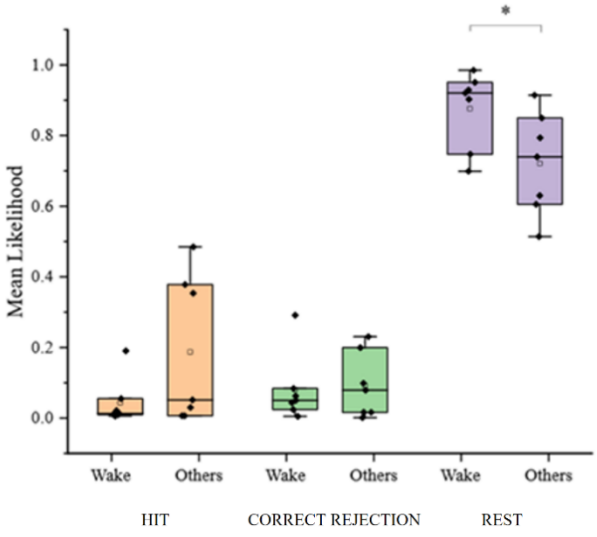

Note. The figure above displays the average activation likelihood of HIT, CORRECT REJECTION, and REST states for seven participants. W represents wake stage, while others represent all other sleep stages (including N1, N2, N3, and REM).

The above results indicate three conclusions: (1) Compared to the other two states, REST has the highest average likelihood; within the REST state, its likelihood during wake was significantly higher

than during other stages; (2) During sleep stages, the average activation likelihood of HIT state is greater than CORRECT REJECTION; (3) Regardless of sleep onset, the average likelihood of CORRECT REJECTION was the lowest among the three states.

Memory Reactivation during the N3 stage

Fig. 3.3 depicts the likelihood of HIT and CORRECT REJECTION states across different sleep stages for seven participants. Using brain states (HIT, CORRECT REJECTION) and sleep stages (W, N1, N2, N3) as within-subject factors, a repeated measures analysis of variance was conducted on the likelihoods of each state. The result shows that the mean likelihood of HIT during N3 sleep is higher than the likelihood of CORRECT REJECTION during N3 and HIT during W periods. This phenomenon indicated a trend where the likelihood of memory reactivation during N3 sleep was higher than that of non-memory control states and higher than during W periods. However, there were no significant effects observed for each sleep stage, both states and their interaction, possibly due to substantial individual differences among participants.

Figure 0.3 The Distribution of HIT and CORRECT REJECTION Likelihood across the Four Sleep Stages

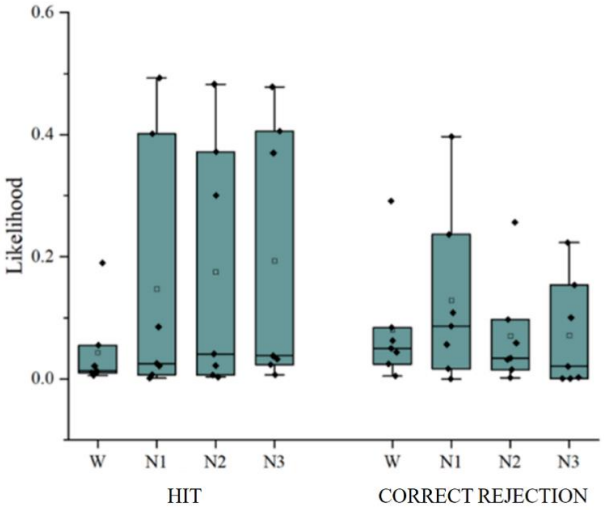

Note. No significant differences were found in the likelihood of the same state occurring across different sleep stages, nor in the likelihood of different states occurring within the same sleep stage.

Figure 0.4 The Distribution of Different State Likelihood across Each Scanning Sequence in the Four Sleep Stages for each participant

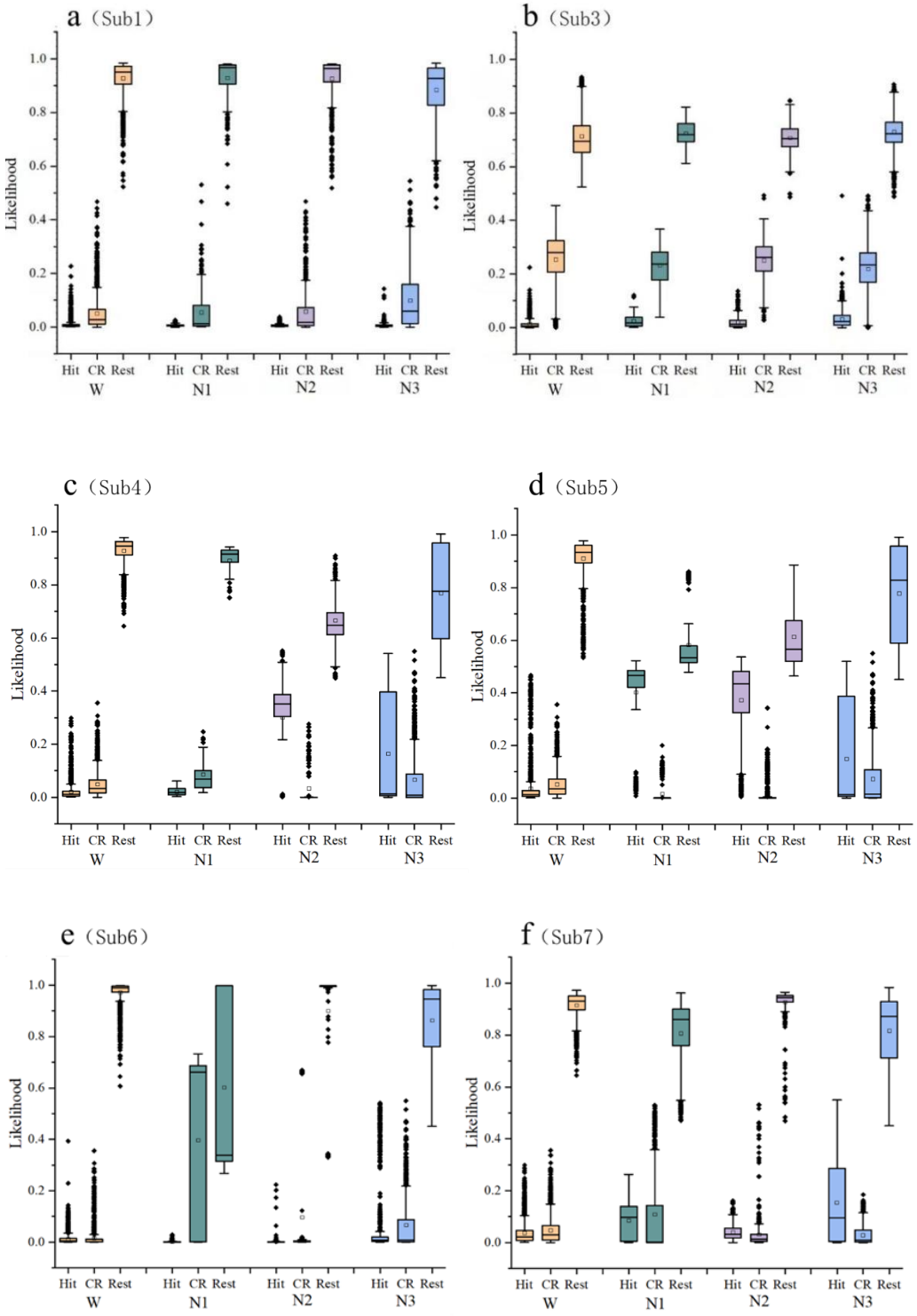

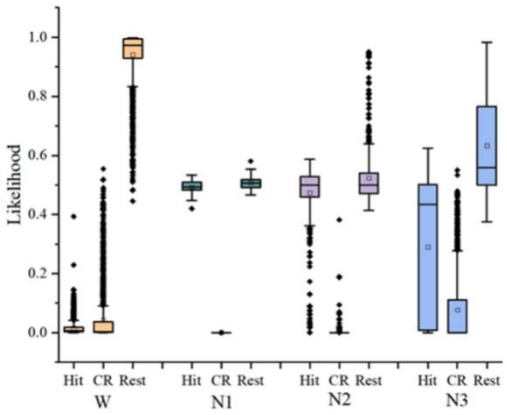

Note. 4 participants (Subjects 4, 5, 7, and 9) had higher average likelihoods of being evaluated as HIT compared to CORRECT REJECTION during scanning sequences in the N3 and N2 stages.

Fig. 3.4 shows the likelihood of three states for each participant across four sleep stages in each scan sequence. Comparisons among participants revealed that 4 out of 7 participants showed significantly higher likelihoods of the HIT state during N3 stages compared to CORRECT REJECTION. This finding suggests that the likelihood of memory reactivation during the N3 stage was higher compared to control states, aligning with the hypothesis of this study. Interestingly, these four participants also showed higher likelihoods of the HIT state during the N2 stage compared to CORRECT REJECTION. This was unexpected, but not contradictory.

To further explore the data, the likelihood for each state was normalized across each participant. Specifically, the mean and standard deviation of the 3000 data points representing the likelihood for each state were calculated, and each data point was transformed into a Z-score by subtracting the mean and dividing by the standard deviation. This normalization approach minimizes differences between states and emphasizes differences within states over time, highlighting points with relatively higher likelihoods during the scan process and enhancing differentiation between different time points. This methodological approach applies consistently across all sleep stages (W, N1, N2, N3), enabling the exploration of likelihood characteristics across different states over time.

Fig. 3.5 displays the average Z-scores of HIT and CORRECT REJECTION across different sleep

stages for the seven participants after normalization. Mann-Whitney U test results indicated: that the HIT state had significantly higher average scores during N2 compared to Wake (Mann-Whitney U=6, P=0.017), and significantly higher scores during N3 compared to Wake (Mann-Whitney U=3, P=0.004). There were no significant differences in HIT scores between other pairs of state sleep stages. In contrast, for the CORRECT REJECTION state, scores did not significantly differ across sleep stages, with a trend towards lower distribution in N2 and N3 compared to the Wake and N1 stages. These findings indicate that, unlike the distribution pattern of control states, the pattern of memory reactivation shows significantly higher activation levels during deeper sleep stages (N3, N2) compared to wakefulness, supporting the hypothesis of this study.

Figure 0.5. The Z-scores of the Two States Normalized across Each Sleep Stage.

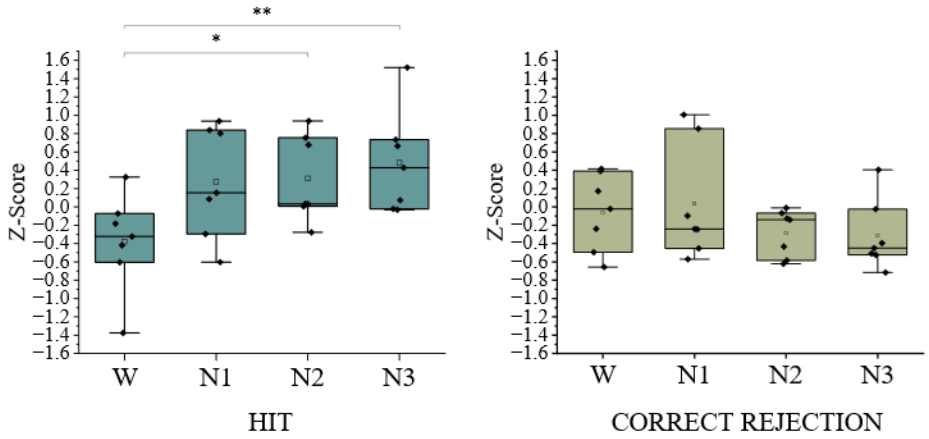

Note. The left figure shows the Z-scores of the HIT state across four sleep stages for 7 participants, with scores in the N3 and N2 stages significantly higher than in the W stage. In contrast, the CORRECT REJECTION state (right figure) did not show this pattern.

Relationship between Memory Reactivation Likelihood and Behavioral Accuracy

To investigate the impact of memory replay on memory performance, the relationship between the likelihood of the HIT state during each stage and the change in memory accuracy before and after sleep was tested (Fig 3.6). A significant negative correlation was revealed between changes in memory

accuracy overnight and the likelihood of HIT during the W stage (rho=-0.762, p=0.046), while the correlation between memory accuracy and HIT likelihood of the other three stages was not significant (N1: rho=-0.232, p=0.617; N2: rho=-0.076, p=0.871; N3: rho=-0.034, p=0.943).

Figure 0.6. The Relationship between HIT likelihood in W state and the Change in Memory Accuracy for the Seven Participants

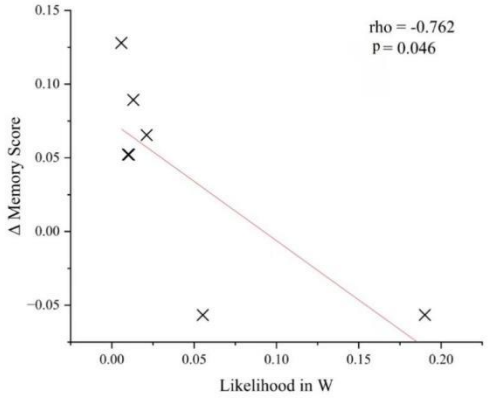

Note. Each cross in the figure represents the relationship between the W state HIT activation likelihood and the change in accuracy of the object-location task before and after sleep for each participant. There are two overlapping points in the [0.01, 0.05] range.

Behavioral Results

First, the accuracy of the object-location memory task was initially analyzed across three stages over two days. Accuracy was calculated as the number of pictures in correct positions over the total number of items in one session (56). Overall, the average accuracy showed a gradual increase across the three stages: the average accuracy in the first stage was 0.615, which improved to 0.814 in the second stage following one practice session, and further increased to 0.853 in the third stage on the second day. Session 2 and Session 3 showed significant improvement compared to Session 1 (Fig 3.7).

Figure 0.7. Changes in Accuracy of Object-Location Memory Across Three Sessions

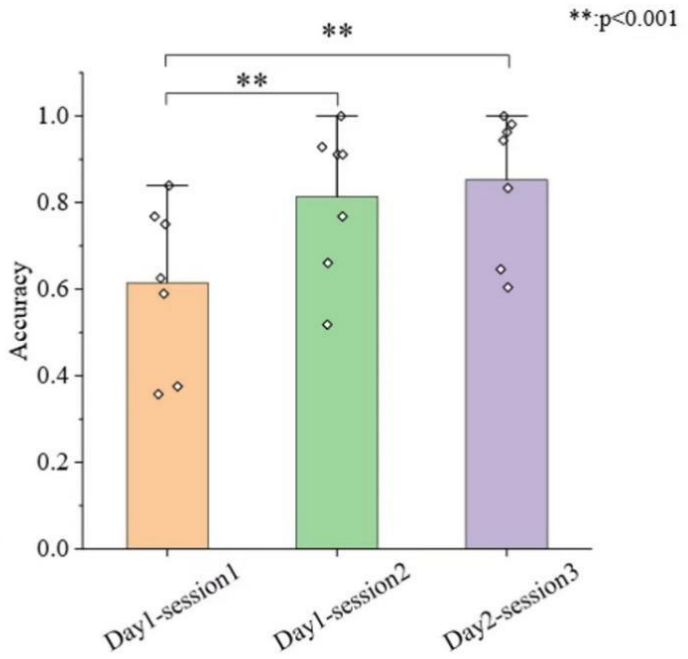

Second, Table 3.2 shows the performance of all participants in the old-new recognition task. Among all the indexes, the hit rate was the proportion of actual old items that were correctly identified as old. Miss rate was the proportion of actual old items that were incorrectly identified as new. The correct rejection rate was the proportion of actual new items that were correctly identified as new. The false alarm rate was the proportion of actual new cases that were incorrectly identified as old. Accuracy was calculated as the correct item numbers (sum of hit items and correct rejection items), reflecting the overall correctness of the system's classifications across all cases. The average data indicated that participants generally had good accuracy in the old-new memory recognition task, with high hit rates, low miss rates, low false alarm rates, and high correct rejection rates. The differences in D-prime values reflect the variability in participants' sensitivity to recognizing old and new stimuli in the task. Some participants performed excellently (e.g., Sub3), while others performed relatively poorly (e.g., Sub1 and Sub5).

Table 0.2. Index for Old-new Recognition Task

	Hit Rate	Miss Rate	False Alarm Rate	Correct Rejection Rate	Accuracy	D-prime
Sub1	0.64	0.36	0.25	0.75	0.70	1.04
Sub3	0.96	0.04	0.04	0.96	0.96	3.61
Sub4	0.86	0.14	0.18	0.82	0.84	1.99
Sub5	0.86	0.12	0.37	0.64	0.75	1.39
Sub6	0.93	0.07	0.13	0.88	0.91	2.62
Sub7	0.95	0.05	0.16	0.84	0.90	2.60
Sub9	0.73	0.27	0.09	0.91	0.82	1.97
Mean	0.85	0.15	0.17	0.83	0.84	2.17

Additionally, as shown in Fig. 3.8, there was a significant correlation between the accuracy of the object-location retrieval memory and old-new recognition memory tasks (tau = 0.81, p = 0.01), which appears that the two different types of memory were behaviorally related.

Figure 0.8 Correlation of Accuracy Between Two Memory Tasks

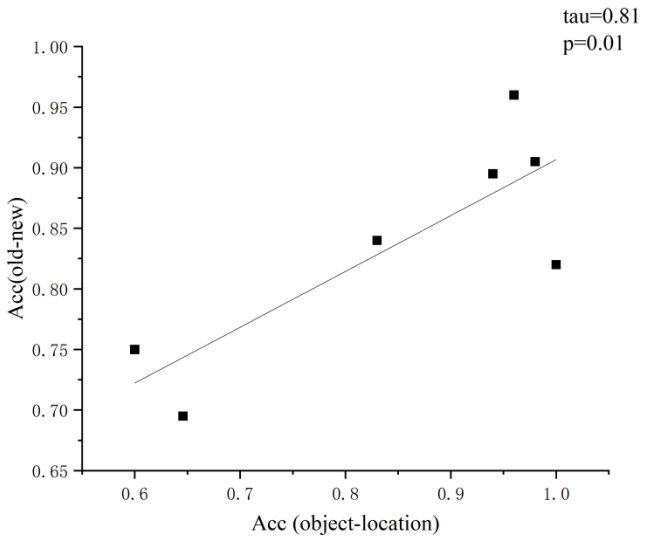

Discussion

This study recruited 11 healthy participants, with criteria including physical condition and sleep quality. Sleep and mental states were assessed through questionnaires to ensure the reliability of the experiment. Two types of memory tasks were designed: an old-new recognition task and an object-location memory task. The old-new recognition task corresponded to the recognition process of objects, while the object-location memory task involved the learning, immediate recall, and delayed recall processes of visual-spatial memory. The main experiment phases included pre-sleep, sleep, and post-sleep stages. Before sleep, participants performed the location encoding task and immediate recall task; after sleep, they performed the old-new recognition task and delayed recall task, with fMRI data collected simultaneously. During sleep, 100 minutes of fMRI-EEG data were collected.

Model Training, Performance and Interpretability

The MVPA method used in this study is innovative in defining memory reactivation states and control states during sleep. The dataset contains three types of samples: HIT state, which represents the correct recognition of old items and is defined as the memory reactivation state, the target pattern of this study; CORRECT REJECTION, which represents the correct recognition of new items; and REST data, obtained from the initial 40 whole brain scans of the wakeful resting state at the beginning of the sleep stage. HIT and CORRECT REJECTION data come from the sequence in the old-new memory data corresponding to the closest whole-brain scan to the peak of the HRF function. Instead of using memory type as a classification standard to reveal reactivation priorities between different memory types (Schapiro et al., 2018; Sterpenich et al., 2021), this approach emphasizes the distinction between memory states and other states during sleep.

The model training workflow of MVPA has several notable advantages. Firstly, it excels in feature processing capabilities. By using templates of memory retrieval-related regions obtained from meta-analysis and the ANOVA-SVM method for training the mask, this method effectively extracts brain

activity features related to memory reactivation, selecting the most significantly activated voxels within each label, and applying weighted processing using the SVM classifier, further enhancing the representativeness and accuracy of the features. Secondly, the method is relatively efficient in both feature extraction and model training. By selecting 500 voxels as the final feature mask during the feature extraction phase, the dimensionality of the data is reduced, thereby improving the efficiency of model training. Thirdly, the method achieved high accuracy and AUC metrics in cross-validation, reflecting the model's accuracy and robustness in brain state evaluation. The accuracy and AUC obtained in cross-validation indicate the model's high predictive power and stability.

However, due to the complexity of neural data and the relatively small number of training samples, the model may be prone to overfitting. It is important to note, though, that the goal of model training is for the study of sleep memory reactivation within the same individuals, rather than generalizing to other datasets. Therefore, although overfitting is a potential issue, it is not particularly severe. Individual thought patterns and corresponding brain activation patterns vary, making the accuracy and stability of the model within individuals more crucial.

In the trained model, hippocampal activation was observed in 6 out of 7 participants, with two participants showing a higher activation proportion in the hippocampus mask compared to other regions. When the hippocampus is used as a template for the same training steps, the cross-validation average accuracy for all participants is relatively high, but the HIT and CORRECT REJECTION categories' accuracy is low for some participants. These two observations suggest that the hippocampus indeed participates in the memory reactivation process, but the degree of involvement varies among participants. The hippocampus is a key area for memory (Voss, Bridge, Cohen, & Walker, 2017), while visual-spatial memory is a complex cognitive and neural process involving the co-activation of many voxels across multiple brain regions (Ayzenberg & Behrmann, 2022; Ladenbauer et al., 2017; Rolls et al., 2022; Swisher et al., 2007). These findings support the role of the hippocampus in visual-spatial memory

and highlight the involvement of multiple brain regions.

Randomizing labels can disrupt the intrinsic structure of the data, making it impossible for the model to extract meaningful patterns and features from the data effectively. This approach provides an important means to verify the robustness of the model. By comparing the model's performance before and after shuffling the labels, we can assess whether the model has truly learned the intrinsic patterns of the data or merely memorized specific training samples. We randomly shuffled the model's labels to construct a meaningless dataset. After shuffling, the model's learning ability significantly decreased. This phenomenon proves that the original dataset has clear and independent boundaries between the three categories, and the model indeed captured the features of each category during training.

Overall Analysis of Sleep Stages and Brain States

Participants who reached N3 sleep had significantly higher scores on the ESS scale, suggesting that higher sleepiness levels may be linked to easier entry into deep sleep. It is generally believed that excessive daytime sleepiness is detrimental to nighttime sleep quality, but it is worth noting that all subjects' levels of sleepiness were within normal ranges. This phenomenon may be related to individuals having higher intrinsic fatigue levels or heightened sleep pressure. Heightened sleep pressure might facilitate the transition into SWS, which is essential for physical and cognitive recovery (Deboer, 2018).

The overall situation of memory activation during different sleep stages shows that among all participants, REST likelihood was the highest among the three conditions. However, there was a varying degree of decline after entering sleep, which aligns with the expectations of this study. Compared to the REST state, its likelihood during wakefulness was significantly higher than during sleep stages. The general statistics across sleep and wakefulness stages indicate that during sleep stages, the average likelihood of HIT activation was greater than CORRECT REJECTION; regardless of sleep onset, the average likelihood of CORRECT REJECTION was the lowest among the three states. These conclusions are consistent with the assumptions made during model establishment, indicating that the brain is in a

resting state before sleep onset, but shows a higher likelihood of entering memory reactivation states after sleep initiation. This supports the efficacy of the model in applying fMRI data during sleep.

Both N2 and N3 sleep stages show priority of memory reactivation.

Based on the EEG data determining sleep stages, statistical analysis of the likelihood distribution of HIT and CORRECT REJECTION states across different sleep stages did not reveal significant differences, possibly due to substantial variability among participants. However, individual comparisons showed that in the N3 and N2 stages, some participants exhibited a higher likelihood of HIT states compared to CORRECT REJECTION states. To further explore the data, likelihood sequences for each participant and state were normalized. Results indicated that in the N2 and N3 stages, Z-scores for HIT states were significantly higher than those for W states, while the distribution of Z-scores for CORRECT REJECTION states did not show this pattern. Overall, these findings support the initial hypothesis that sleep stage N3, characterized by slow-wave sleep, has a greater likelihood of memory reactivation.

It is noteworthy that besides the N3 stage, Z-scores for HIT states in the N2 stage also significantly differed from those in the W stage. This may be because, similar to N3, N2 stages also exhibit some slow-wave activity (Berry et al., 2017). Additionally, N2 stages are characterized by a high occurrence of spindles, which are closely related to memory reactivation (Laventure et al., 2018). Spindles reaching the neocortex during sleep may facilitate the activation of respective neural networks, potentially through stimulating calcium influx and subsequent synaptic plasticity processes. The memory information carried within spindle oscillations may play a crucial role in altering synaptic connections for long-term information storage within respective neocortical networks.

During wakefulness, reactivation may impact memory consolidation.

The relationship between memory reactivation likelihood during wakefulness and nighttime memory accuracy revealed a negative correlation. This suggests that memory reactivation during wakefulness may impair memory performance. Unlike the reactivation occurring during offline SWS,

wakeful reactivation may render memories unstable and susceptible to interference, which is consistent with previous studies. In one study, rats underwent memory training followed by memory reactivation through electrical stimulation during either SWS or wakefulness. The study found that reactivation imposed during SWS enhanced subsequent memory strength, whereas similar reactivation during wakefulness induced memory loss (Barnes & Wilson, 2014). In another human study, olfactory cues were used to reactivate memories (Rasch, Büchel, Gais, & Born, 2007). Participants learned the locations of card pairs in the presence of a specific odor cue. Later, the odor was re-exposed to reactivate memories during either SWS or wakefulness. Following odor cue reactivation, participants immediately underwent interference learning (learning card pairs in different locations) as a disruption task, followed by a final test to assess memory retention. In the final retrieval test, when interference learning occurred during wakefulness, participants' memory of the initial card positions was significantly impaired. In contrast, during SWS, odor cue-triggered memory reactivation stabilized memories. Despite interference learning following reactivation, participants showed better memory retention of the original card positions in the final retrieval test compared to control conditions (without memory reactivation during SWS).

The above phenomena can be explained by synaptic plasticity and the synaptic homeostasis hypothesis. SOs during SWS synchronize neuronal activity, enhancing connections between neurons. This synchronization helps coordinate neural network activity, making synaptic connections more stable, thereby promoting memory reconsolidation (Rasch & Born, 2013). Additionally, during SWS, synaptic downscaling occurs, weakening weaker synaptic connections. This process helps eliminate unnecessary neural connections, maintaining brain stability and energy balance while strengthening useful synaptic connections. Synaptic downscaling enhances the efficiency of neural networks, optimizing memory consolidation(Haubrich & Nader, 2018; Tononi & Cirelli, 2019). However, the mechanism can also lead to reduced memory in some cases. When memories are retrieved or reactivated, they enter a

transiently unstable state. During this unstable state, synapses related to memory become more plastic (Haubrich & Nader, 2018; J. L. C. Lee, Nader, & Schiller, 2017). If this reactivation occurs during wakefulness, memories are susceptible to external interference and modification. Correspondingly, when reactivation occurs during the N3 stage, memories undergo rapid reconsolidation due to communication mechanisms between the hippocampus and cortex during SWS (Diekelmann, Büchel, Born, & Rasch, 2011; Stickgold & Walker, 2005).

These phenomena underscore the irreplaceable role of SWS in memory consolidation by enhancing synaptic plasticity and stability, ensuring the persistence and accuracy of memories. Here, however, changes in memory performance did not show a positive correlation with representations of memory reactivation during N3. This may come from participant's differences in sleep architecture, such as the proportion of time spent in N3 sleep in different individuals, which could introduce variability that obscures a clear correlation. Since the average likelihood of memory reactivation during N3 is estimated here, considering that some subjects have a short N3 duration, although this period has a higher likelihood of reactivation, the overall memory consolidation effect is not strong. In this regard, more in-depth exploration may be needed.

Behavioral performance of item memory and context memory are correlated.

The results of the object-location memory task showed a significant increase in accuracy from the first to the second and third stages. The significant rise in memory accuracy from the first to the second stage indicates that participants gradually mastered the task, showing good compliance. Although the accuracy improvement from the second to the third stage was not significant, likely due to insufficient sample size, the overall upward trend in mean accuracy suggests that sleep did not lead to accelerated forgetting, highlighting the stabilizing effect of sleep on memory.

In object-location memory tasks, behavioral accuracy tended to improve along the course of the experiment, supporting the positive effects of training and sleep on memory performance. In the old-

new memory task, participants generally exhibited high accuracy, hit rates, and correct rejection rates. The d-prime values indicated significant individual differences in the ability to distinguish between target and non-target stimuli. Nonetheless, all d-prime values were above 1, which is within the normal range (Macmillan & Creelman, 2005).

The accuracy of item memory was correlated with context memory, aligning with previous theoretical research and our expectations. The high correlation between the two memory tasks (tau = 0.81) suggests that they might share similar cognitive and neural mechanisms. Some theories propose that the hippocampus integrates item and context information into an episodic memory trace during memory encoding (Zimmer & Ecker, 2010). This phenomenon may also reflect the brain's ability to integrate objects with their contextual information during memory processing and storage, implying that individuals who can accurately remember the location of objects are also more likely to accurately recognize old and new objects (Ford, Verfaellie, & Giovanello, 2010; Guo, Shubeck, & Hu, 2021).

Limitations

Despite the rigorous and scientific work done in the experimental design, data analysis, and theoretical support of this paper, there are still some shortcomings and limitations, mainly including the following three points:

Small sample size: Due to experimental conditions, the final number of participants included in the experiment was small, which may lead to false negatives or false positives. For example, when analyzing the likelihood distributions of HIT and CORRECT REJECTION states in different sleep stages, direct repeated measures ANOVA only showed trends without significance; in the analysis of the correlation between HIT likelihood and memory score changes in the Wake stage, due to the small sample size, there may be accidental correlations.

Incomplete sleep data: Participants had to be awakened after data collection, which may have affected the accurate reflection of the overall sleep structure. Additionally, some participants had short

SWS durations, and REM sleep only appeared in a few participants.

Lack of control variables: The experiment did not control for participants' physical activity, which may have impacted sleep and memory results. The lack of an adaptation night might have caused participants to have poorer sleep quality due to unfamiliarity with the environment during the experimental night, reducing the validity of the experimental data or causing the results to be influenced by unusual changes due to the unfamiliar environment.

Conclusions

This study primarily investigates the relationship between visual-spatial memory and sleep. The main work includes three parts: (1) Experimental design and data collection, (2) Memory reactivation model based on MVPA methods, and (3) Results of memory reactivation during sleep. Through the above steps, two main conclusions are drawn: (1) Both N2 and N3 sleep stages show priority of memory reactivation. (2) During wakefulness, reactivation may impact memory consolidation.

In the first part, a series of memory tasks were designed to test the associative memory of objects and spatial locations, as well as the recognition memory of objects themselves (old-new recognition). fMRI data were collected during the memory tasks, and fMRI-EEG synchronized data were collected during sleep. The experimental design, incorporating previous research, cleverly balanced the two types of memory. Behavioral performance in object-location memory demonstrated participant compliance and the stability of memory before and after sleep. In the old-new recognition memory task, overall behavioral performance was high, but there were significant differences in signal detection sensitivity among participants. Moreover, the experimental results showed that the behavioral accuracy of the two tasks was correlated, suggesting that they might share similar cognitive and neural mechanisms.

In the second part, a three-class machine learning model was trained using the HIT and CORRECT REJECTION sequences in the old-new recognition memory task and the resting-state data with

eyes closed before sleep. HIT was used to predict memory reactivation, CORRECT REJECTION corresponded to the control for novel stimuli, and REST represents close-eye control activity. The model was trained using three groups as the training set and one group as the test set, with cross-validation showing good accuracy and area AUC performance. Additionally, the role of the hippocampus in feature classification was analyzed, along with the model's performance after data shuffling, demonstrating the physiological significance of the model. This model, with balanced samples, exhibited good feature processing capabilities, accuracy, robustness, and interpretability, effectively distinguishing memory reactivation from control groups, and facilitating the accurate identification of various patterns during sleep.

The third part mainly presented the activation results obtained from the MVPA model during sleep, correlating the estimated brain states with different sleep stages based on detailed sleep EEG analysis. During the wakeful pre-sleep stage, the likelihood of the REST state was higher, indicating that the model could reflect the resting control state, supporting its validity in sleep stages. Statistical analysis of the likelihood distribution of the other two states across different sleep stages did not show significant differences, possibly due to large individual differences among participants. However, individual comparisons showed that some participants had a significantly higher likelihood of HIT state compared to the CORRECT REJECTION state during the N3 and N2 stages. Further normalization of the likelihood sequences for each participant in each state reduced individual differences and emphasized temporal distribution differences within each state. It was found that during the N2 and N3 stages, the Z-scores for the HIT state were significantly higher than during the wakefulness period, while the distribution of CORRECT REJECTION did not show this pattern. This supports the initial hypothesis of the study that memory reactivation is more likely to occur during SWS (N3 stage). Additionally, behavioral data and their association with activation were analyzed, showing a negative correlation between the activation likelihood of the HIT pattern during the wakeful stage and the change in participants'

performance from the first to the second stage, supporting that memory reactivation during wakefulness can affect the stability of memory consolidation.

In conclusion, this study, through four main parts, deeply explores the relationship between visual-spatial memory and sleep. By designing experiments, training memory reactivation models, applying MVPA models to sleep data analysis, and integrating sleep EEG data, it demonstrates that memory reactivation is more likely to occur during SWS (N3 stage). The methods used in this study effectively adapt to the complexity and non-linear characteristics of visual-spatial memory reactivation, accurately pinpointing the timing of memory reactivation from sleep fMRI sequences, providing strong evidence for the active systems consolidation hypothesis of memory, and adding more details. This study offers important empirical support for understanding the complex relationship between memory and sleep and provides theoretical and methodological references for future research in this field.

Reference

Abraham, A., Pedregosa, F., Eickenberg, M., Gervais, P., Mueller, A., Kossaifi, J., … Varoquaux, G. (2014). Machine learning for neuroimaging with scikit-learn. *Frontiers in Neuroinformatics*, *8*. https://doi.org/10.3389/fninf.2014.00014

Adamantidis, A. R., Gutierrez Herrera, C., & Gent, T. C. (2019). Oscillating circuitries in the sleeping brain. *Nature Reviews. Neuroscience*, *20*, 746–762.

Almeida-Filho, D. G., Queiroz, C. M., & Ribeiro, S. (2018). Memory corticalization triggered by REM sleep: Mechanisms of cellular and systems consolidation. *Cellular and Molecular Life Sciences*, *75*, 3715–3740.

Antony, J. W., Piloto, L., Wang, M., Pacheco, P., Norman, K. A., & Paller, K. A. (2018). Sleep spindle refractoriness segregates periods of memory reactivation. *Current Biology : CB*, *28*, 1736-1743.e4.

Ayzenberg, V., & Behrmann, M. (2022). The Dorsal Visual Pathway Represents Object-Centered Spatial Relations for Object Recognition. *The Journal of Neuroscience: The Official Journal of the Society for Neuroscience*, *42*, 4693–4710.

Azimi, A., Alizadeh, Z., & Ghorbani, M. (2021). The essential role of hippocampo-cortical connections in temporal coordination of spindles and ripples. *NeuroImage*, *243*, 118485.

Ba, M., V, R., B, L., Jm, S., Jr, L., S, A.-I., … Mp, W. (2013). Prefrontal atrophy, disrupted NREM slow waves and impaired hippocampal-dependent memory in aging. *Nature Neuroscience*, *16*. https://doi.org/10.1038/nn.3324

Babu, U. M., & Ganesan, K. (2020). *EFFECTIVENESS OF VISUAL-SPATIAL SKILLS TO ENHANCING THE LONG TERM MEMORY OF GIFTED SECONDARY STUDENTS*.

Baddeley, A. D. (1990). The development of the concept of working memory: Implications and contributions of neuropsychology. In *Neuropsychological impairments of short-term memory.* (pp. 54–

73). New York, NY, US: Cambridge University Press.

Barnes, D. C., & Wilson, D. A. (2014). Slow-wave sleep-imposed replay modulates both strength and precision of memory. *The Journal of Neuroscience: The Official Journal of the Society for Neuroscience*, *34*, 5134–5142.

Bergmann, T. O., Mölle, M., Diedrichs, J., Born, J., & Siebner, H. R. (2012). Sleep spindle-related reactivation of category-specific cortical regions after learning face-scene associations. *NeuroImage*, *59*, 2733–2742.

Berry, R. B., Brooks, R., Gamaldo, C., Harding, S. M., Lloyd, R. M., Quan, S. F., … Vaughn, B. V. (2017). AASM Scoring Manual Updates for 2017 (Version 2.4). *Journal of Clinical Sleep Medicine: JCSM: Official Publication of the American Academy of Sleep Medicine*, *13*, 665–666.

Blumberg, M. S., Lesku, J. A., Libourel, P.-A., Schmidt, M. H., & Rattenborg, N. C. (2020). What Is REM Sleep? *Current Biology*, *30*, R38–R49.

Born, J., & Wilhelm, I. (2012). System consolidation of memory during sleep. *Psychological Research*, *76*, 192–203.

Boutin, A., Pinsard, B., Boré, A., Carrier, J., Fogel, S. M., & Doyon, J. (2018). Transient synchronization of hippocampo-striato-thalamo-cortical networks during sleep spindle oscillations induces motor memory consolidation. *NeuroImage*, *169*, 419–430.

Brodt, S., Inostroza, M., Niethard, N., & Born, J. (2023). Sleep—A brain-state serving systems memory consolidation. *Neuron*, *111*, 1050–1075.

Brodziak, A., Brewczyński, A., & Bajor, G. (2013). Clinical significance of knowledge about the structure, function, and impairments of working memory. *Medical Science Monitor : International Medical Journal of Experimental and Clinical Research*, *19*, 327–338.

Buck, S., Bastos, F., Baldeweg, T., & Vargha-Khadem, F. (2021). The Pair Test: A computerised measure of learning and memory. *Behavior Research Methods*, *53*, 928–942.

Buzsáki, G. (2015). Hippocampal sharp wave-ripple: A cognitive biomarker for episodic memory and planning. *Hippocampus*, *25*, 1073–1188.

Clawson, B. C., Pickup, E. J., Ensing, A., Geneseo, L., Shaver, J., Gonzalez-Amoretti, J., … Aton, S. J. (2021). Causal role for sleep-dependent reactivation of learning-activated sensory ensembles for fear memory consolidation. *Nature Communications*, *12*, 1200.

Connolly, A. C., Guntupalli, J. S., Gors, J., Hanke, M., Halchenko, Y. O., Wu, Y.-C., … Haxby, J. V. (2012). The Representation of Biological Classes in the Human Brain. *Journal of Neuroscience*, *32*, 2608–2618.

Davidson, T. J., Kloosterman, F., & Wilson, M. A. (2009). Hippocampal replay of extended experience. *Neuron*, *63*, 497–507.

Deboer, T. (2018). Sleep homeostasis and the circadian clock: Do the circadian pacemaker and the sleep homeostat influence each other's functioning? *Neurobiology of Sleep and Circadian Rhythms*, *5*, 68–77.

Denis, D., & Cairney, S. A. (2023). Neural reactivation during human sleep. *Emerging Topics in Life Sciences*, *7*, 487–498.

Denis, D., Mylonas, D., Poskanzer, C., Bursal, V., Payne, J. D., & Stickgold, R. (2021). Sleep Spindles Preferentially Consolidate Weakly Encoded Memories. *The Journal of Neuroscience: The Official Journal of the Society for Neuroscience*, *41*, 4088–4099.

Deuker, L., Olligs, J., Fell, J., Kranz, T. A., Mormann, F., Montag, C., … Axmacher, N. (2013). Memory Consolidation by Replay of Stimulus-Specific Neural Activity. *The Journal of Neuroscience*, *33*, 19373–19383.

Diana, R. A., Yonelinas, A. P., & Ranganath, C. (2007). Imaging recollection and familiarity in the medial temporal lobe: A three-component model. *Trends in Cognitive Sciences*, *11*, 379–386.

Diba, K., & Buzsáki, G. (2007). Forward and reverse hippocampal place-cell sequences during

ripples. *Nature Neuroscience*, *10*, 1241–1242.

Dickerson, B. C., & Eichenbaum, H. (2010). The Episodic Memory System: Neurocircuitry and Disorders. *Neuropsychopharmacology*, *35*, 86–104.

Diekelmann, S., Büchel, C., Born, J., & Rasch, B. (2011). Labile or stable: Opposing consequences for memory when reactivated during waking and sleep. *Nature Neuroscience*, *14*, 381–386.

Dockès, J., Poldrack, R. A., Primet, R., Gözükan, H., Yarkoni, T., Suchanek, F., … Varoquaux, G. (2020). NeuroQuery, comprehensive meta-analysis of human brain mapping. *eLife*, *9*, e53385.

Ebrahimi, A. M. (2021). *Panentheism, Spinoza and world religions: Can the panentheistic idea be found in the major world religions?* 27.

Euston, D. R., Tatsuno, M., & McNaughton, B. L. (2007). Fast-forward playback of recent memory sequences in prefrontal cortex during sleep. *Science (New York, N.Y.)*, *318*, 1147–1150.

Fernandez, L. M. J., & Lüthi, A. (2020). Sleep Spindles: Mechanisms and Functions. *Physiological Reviews*, *100*, 805–868.

Flanagin, V. L., Klinkowski, S., Brodt, S., Graetsch, M., Roselli, C., Glasauer, S., & Gais, S. (2023). The precuneus as a central node in declarative memory retrieval. *Cerebral Cortex (New York : 1991)*, *33*, 5981–5990.

Fogel, S., Albouy, G., King, B. R., Lungu, O., Vien, C., Bore, A., … Doyon, J. (2017). Reactivation or transformation? Motor memory consolidation associated with cerebral activation time-locked to sleep spindles. *PLoS ONE*, *12*, e0174755.

Ford, J. H., Verfaellie, M., & Giovanello, K. S. (2010). Neural correlates of familiarity-based associative retrieval. *Neuropsychologia*, *48*, 3019–3025.

Girardeau, G., Benchenane, K., Wiener, S. I., Buzsáki, G., & Zugaro, M. B. (2009). Selective suppression of hippocampal ripples impairs spatial memory. *Nature Neuroscience*, *12*, 1222–1223.

Goldman-Rakic, P. S. (1996). The prefrontal landscape: Implications of functional architecture for

understanding human mentation and the central executive. *Philosophical Transactions of the Royal Society of London. Series B, Biological Sciences*, *351*, 1445–1453.

Guo, J., Shubeck, K., & Hu, X. (2021). Relationship Between Item and Source Memory: Explanation of Connection-Strength Model. *Frontiers in Psychology*, *12*, 691577.

Hahn, M. A., Bothe, K., Heib, D., Schabus, M., Helfrich, R. F., & Hoedlmoser, K. (n.d.). Slow oscillation–spindle coupling strength predicts real-life gross-motor learning in adolescents and adults. *eLife*, *11*, e66761.

Hahn, M. A., Heib, D., Schabus, M., Hoedlmoser, K., & Helfrich, R. F. (n.d.). Slow oscillation-spindle coupling predicts enhanced memory formation from childhood to adolescence. *eLife*, *9*, e53730.

Halonen, R., Kuula, L., Antila, M., & Pesonen, A.-K. (2021). The Overnight Retention of Novel Metaphors Associates With Slow Oscillation–Spindle Coupling but Not With Respiratory Phase at Encoding. *Frontiers in Behavioral Neuroscience*, *15*, 712774.

Haubrich, J., & Nader, K. (2018). Memory Reconsolidation. In R. E. Clark & S. J. Martin (Eds.), *Behavioral Neuroscience of Learning and Memory* (pp. 151–176). Cham: Springer International Publishing.

Haxby, J. V., Gobbini, M. I., Furey, M. L., Ishai, A., Schouten, J. L., & Pietrini, P. (2001). Distributed and overlapping representations of faces and objects in ventral temporal cortex. *Science (New York, N.Y.)*, *293*, 2425–2430.

Haynes, J.-D., & Rees, G. (2005a). Predicting the orientation of invisible stimuli from activity in human primary visual cortex. *Nature Neuroscience*, *8*, 686–691.

Haynes, J.-D., & Rees, G. (2005b). Predicting the Stream of Consciousness from Activity in Human Visual Cortex. *Current Biology*, *15*, 1301–1307.

Helfrich, R. F., Mander, B. A., Jagust, W. J., Knight, R. T., & Walker, M. P. (2018). Old Brains Come Uncoupled in Sleep: Slow Wave-Spindle Synchrony, Brain Atrophy, and Forgetting. *Neuron*, *97*, 221-

230.e4.

Herberger, S., Penzel, T., Fietze, I., Glos, M., Cicolin, A., Fattori, E., … Kräuchi, K. (2024). Enhanced conductive body heat loss during sleep increases slow-wave sleep and calms the heart. *Scientific Reports*, *14*, 4669.

Höller, Y., Eyjólfsdóttir, S., Van Schalkwijk, F. J., & Trinka, E. (2024). The effects of slow wave sleep characteristics on semantic, episodic, and procedural memory in people with epilepsy. *Frontiers in Pharmacology*, *15*. https://doi.org/10.3389/fphar.2024.1374760

Holz, J., Piosczyk, H., Feige, B., Spiegelhalder, K., Baglioni, C., Riemann, D., & Nissen, C. (2012). EEG Σ and slow-wave activity during NREM sleep correlate with overnight declarative and procedural memory consolidation. *Journal of Sleep Research*, *21*, 612–619.

Hu, X., Cheng, L. Y., Chiu, M. H., & Paller, K. A. (2020). Promoting memory consolidation during sleep: A meta-analysis of targeted memory reactivation. *Psychological Bulletin*, *146*, 218–244.

Iber, C., Ancoli-Israel, S., Chesson, A. L., & Quan, S. (2007). The AASM Manual for the Scoring of Sleep and Associated Events: Rules, Terminology and Technical Specifications. *Westchester, IL: American Academy of Sleep Medicine*.

Inostroza, M., & Born, J. (2013). Sleep for preserving and transforming episodic memory. *Annual Review of Neuroscience*, *36*, 79–102.

Isomura, Y., Sirota, A., Ozen, S., Montgomery, S., Mizuseki, K., Henze, D. A., & Buzsáki, G. (2006). Integration and segregation of activity in entorhinal-hippocampal subregions by neocortical slow oscillations. *Neuron*, *52*, 871–882.

Jiang, X., Gonzalez-Martinez, J., & Halgren, E. (2019). Posterior Hippocampal Spindle Ripples Co-occur with Neocortical Theta Bursts and Downstates-Upstates, and Phase-Lock with Parietal Spindles during NREM Sleep in Humans. *Journal of Neuroscience*, *39*, 8949–8968.

Kamitani, Y., & Tong, F. (2005). Decoding the visual and subjective contents of the human brain.

Nature Neuroscience, *8*, 679–685.

Keenan, S., & Hirshkowitz, M. (2017). Chapter 161—Sleep Stage Scoring. In M. Kryger, T. Roth, & W. C. Dement (Eds.), *Principles and Practice of Sleep Medicine (Sixth Edition)* (pp. 1567-1575.e3). Elsevier.

Kesner, R. P. (2009). The posterior parietal cortex and long-term memory representation of spatial information. *Neurobiology of Learning and Memory*, *91*, 197–206.

Klinzing, J. G., Niethard, N., & Born, J. (2019). Mechanisms of systems memory consolidation during sleep. *Nature Neuroscience*, *22*, 1598–1610.

Kolb, B., & Whishaw, I. Q. (2009). *Fundamentals of human neuropsychology* (6th ed). New York, NY: Worth Publishers.

Kubilius, J., Baeck, A., Wagemans, J., & Op de Beeck, H. P. (2015). Brain-decoding fMRI reveals how wholes relate to the sum of parts. *Cortex*, *72*, 5–14.

Ladenbauer, J., Ladenbauer, J., Külzow, N., de Boor, R., Avramova, E., Grittner, U., & Flöel, A. (2017). Promoting Sleep Oscillations and Their Functional Coupling by Transcranial Stimulation Enhances Memory Consolidation in Mild Cognitive Impairment. *The Journal of Neuroscience: The Official Journal of the Society for Neuroscience*, *37*, 7111–7124.

Lansink, C. S., Goltstein, P. M., Lankelma, J. V., Joosten, R. N. J. M. A., McNaughton, B. L., & Pennartz, C. M. A. (2008). Preferential Reactivation of Motivationally Relevant Information in the Ventral Striatum. *The Journal of Neuroscience*, *28*, 6372–6382.

Laventure, S., Pinsard, B., Lungu, O., Carrier, J., Fogel, S., Benali, H., … Doyon, J. (2018). Beyond spindles: Interactions between sleep spindles and boundary frequencies during cued reactivation of motor memory representations. *Sleep*, *41*, zsy142.

Lee, A. K., & Wilson, M. A. (2002). Memory of sequential experience in the hippocampus during slow wave sleep. *Neuron*, *36*, 1183–1194.

Lee, J. L. C., Nader, K., & Schiller, D. (2017). An update on memory reconsolidation updating.

Trends in Cognitive Sciences, *21*, 531–545.

Léger, D., Debellemaniere, E., Rabat, A., Bayon, V., Benchenane, K., & Chennaoui, M. (2018). Slow-wave sleep: From the cell to the clinic. *Sleep Medicine Reviews*, *41*, 113–132.

Li, A. Y. (2021). Object and Spatial Context Representations in Visual Short-Term Memory. *eNeuro*, *8*, ENEURO.0076-21.2021.

Logothetis, N. K., & Wandell, B. A. (2004). Interpreting the BOLD signal. *Annual Review of Physiology*, *66*, 735–769.

Lüthi, A., & McCormick, D. A. (1999). Modulation of a pacemaker current through Ca2+-induced stimulation of cAMP production. *Nature Neuroscience*, *2*, 634–641.

Macmillan, N. A., & Creelman, C. D. (2005). *Detection theory: A user's guide* (2nd ed). Mahwah, N.J: Lawrence Erlbaum Associates.

Malerba, P., & Bazhenov, M. (2019). Circuit mechanisms of hippocampal reactivation during sleep. *Neurobiology of Learning and Memory*, *160*, 98–107.

Massimini, M., Huber, R., Ferrarelli, F., Hill, S., & Tononi, G. (2004). The Sleep Slow Oscillation as a Traveling Wave. *The Journal of Neuroscience*, *24*, 6862–6870.

McAfoose, J., & Baune, B. T. (2009). Exploring visual-spatial working memory: A critical review of concepts and models. *Neuropsychology Review*, *19*, 130–142.

McCarthy, P. (2024, February 16). FslInstallation—FslWiki. Retrieved March 20, 2024, from https://fsl.fmrib.ox.ac.uk/fsl/fslwiki/FslInstallation

Mikutta, C., Feige, B., Maier, J. G., Hertenstein, E., Holz, J., Riemann, D., & Nissen, C. (2019). Phase-amplitude coupling of sleep slow oscillatory and spindle activity correlates with overnight memory consolidation. *Journal of Sleep Research*, *28*, e12835.

Miller, E. K., & Cohen, J. D. (2001). An integrative theory of prefrontal cortex function. *Annual Review of Neuroscience*, *24*, 167–202.

Milner, B., Johnsrude, I., & Crane, J. (1997). Right medial temporal-lobe contribution to object-location memory. *Philosophical Transactions of the Royal Society B: Biological Sciences*, *352*, 1469–1474.

Misaki, M., Kim, Y., Bandettini, P. A., & Kriegeskorte, N. (2010). Comparison of multivariate classifiers and response normalizations for pattern-information fMRI. *NeuroImage*, *53*, 103–118.

Mitchell, T. M., Hutchinson, R., Niculescu, R. S., Pereira, F., Wang, X., Just, M., & Newman, S. (2004). Learning to Decode Cognitive States from Brain Images. *Machine Learning*, *57*, 145–175.

Mölle, M., Marshall, L., Gais, S., & Born, J. (2004). Learning increases human electroencephalographic coherence during subsequent slow sleep oscillations. *Proceedings of the National Academy of Sciences*, *101*, 13963–13968.

Murphy, K. P. (2012). *Machine learning—A probabilistic perspective*. Presented at the Adaptive computation and machine learning series. Retrieved from https://www.semanticscholar.org/paper/Machine-learning-a-probabilistic-perspective-Murphy/360ca02e6f5a5e1af3dce4866a257aafc2d6d6f5

Nayak, C. S., & Anilkumar, A. C. (2024). EEG Normal Sleep. In *StatPearls*. Treasure Island (FL): StatPearls Publishing.

Niethard, N., Ngo, H.-V. v., Ehrlich, I., & Born, J. (2018). Cortical circuit activity underlying sleep slow oscillations and spindles. *Proceedings of the National Academy of Sciences*, *115*, E9220–E9229.

Niknazar, H., Malerba, P., & Mednick, S. C. (2022). Slow oscillations promote long-range effective communication: The key for memory consolidation in a broken-down network. *Proceedings of the National Academy of Sciences of the United States of America*, *119*, e2122515119.

Nir, Y., Staba, R. J., Andrillon, T., Vyazovskiy, V. V., Cirelli, C., Fried, I., & Tononi, G. (2011). Regional Slow Waves and Spindles in Human Sleep. *Neuron*, *70*, 153–169.

Norman, K. A., Polyn, S. M., Detre, G. J., & Haxby, J. V. (2006). Beyond mind-reading: Multi-voxel pattern analysis of fMRI data. *Trends in Cognitive Sciences*, *10*, 424–430.

Oliva, A., Fernández-Ruiz, A., Buzsáki, G., & Berényi, A. (2016). Role of Hippocampal CA2 Region in Triggering Sharp-Wave Ripples. *Neuron*, *91*, 1342–1355.

O'Neill, J., Pleydell-Bouverie, B., Dupret, D., & Csicsvari, J. (2010). Play it again: Reactivation of waking experience and memory. *Trends in Neurosciences*, *33*, 220–229.

Patel, A. K., Reddy, V., Shumway, K. R., & Araujo, J. F. (2024). Physiology, Sleep Stages. In *StatPearls*. Treasure Island (FL): StatPearls Publishing.

Patel, J., Schomburg, E. W., Berényi, A., Fujisawa, S., & Buzsáki, G. (2013). Local Generation and Propagation of Ripples along the Septotemporal Axis of the Hippocampus. *The Journal of Neuroscience*, *33*, 17029–17041.

Pedregosa, F., Varoquaux, G., Gramfort, A., Michel, V., Thirion, B., Grisel, O., … Duchesnay, É. (2011). Scikit-learn: Machine Learning in Python. *Journal of Machine Learning Research*, *12*, 2825–2830.

Peelen, M. V., & Downing, P. E. (2023). Testing cognitive theories with multivariate pattern analysis of neuroimaging data. *Nature Human Behaviour*, *7*, 1430–1441.

Peigneux, P., Laureys, S., Fuchs, S., Collette, F., Perrin, F., Reggers, J., … Maquet, P. (2004). Are spatial memories strengthened in the human hippocampus during slow wave sleep? *Neuron*, *44*, 535–545.

Pereira, F., Mitchell, T., & Botvinick, M. (2009). Machine learning classifiers and fMRI: A tutorial overview. *NeuroImage*, *45*, S199–S209.

Platt, J. (2000). Probabilistic Outputs for Support Vector Machines and Comparisons to Regularized Likelihood Methods. *Adv. Large Margin Classif.*, *10*.

Polyn, S. M., Natu, V. S., Cohen, J. D., & Norman, K. A. (2005). Category-Specific Cortical Activity Precedes Retrieval During Memory Search. *Science*, *310*, 1963–1966.

Qin Y. (2020). *Fusion of EEG rhythm and magnetic resonance information and its application in the study of epilepsy* (Doctoral dissertation, University of Electronic Science and Technology of China).

University of Electronic Science and Technology of China.

Rasch, B., & Born, J. (2013). About sleep's role in memory. *Physiological Reviews*, *93*, 681–766.

Rasch, B., Büchel, C., Gais, S., & Born, J. (2007). Odor cues during slow-wave sleep prompt declarative memory consolidation. *Science (New York, N.Y.)*, *315*, 1426–1429.

Rolls, E. T., Deco, G., Huang, C.-C., & Feng, J. (2022). The human posterior parietal cortex: Effective connectome, and its relation to function. *Cerebral Cortex (New York, NY)*, *33*, 3142–3170.

Romanski, L. M. (2004). Domain specificity in the primate prefrontal cortex. *Cognitive, Affective & Behavioral Neuroscience*, *4*, 421–429.

Rosanova, M., & Ulrich, D. (2005). Pattern-Specific Associative Long-Term Potentiation Induced by a Sleep Spindle-Related Spike Train. *The Journal of Neuroscience*, *25*, 9398–9405.

Rothschild, G., Eban, E., & Frank, L. M. (2017). A cortical–hippocampal–cortical loop of information processing during memory consolidation. *Nature Neuroscience*, *20*, 251–259.

Rudoy, J. D., Voss, J. L., Westerberg, C. E., & Paller, K. A. (2009). Strengthening individual memories by reactivating them during sleep. *Science (New York, N.Y.)*, *326*, 1079.

Sadowski, J. H. L. P., Jones, M. W., & Mellor, J. R. (2016). Sharp-Wave Ripples Orchestrate the Induction of Synaptic Plasticity during Reactivation of Place Cell Firing Patterns in the Hippocampus. *Cell Reports*, *14*, 1916–1929.

Saeys, Y., Inza, I., & Larrañaga, P. (2007). A review of feature selection techniques in bioinformatics. *Bioinformatics (Oxford, England)*, *23*, 2507–2517.

Schapiro, A. C., McDevitt, E. A., Rogers, T. T., Mednick, S. C., & Norman, K. A. (2018). Human hippocampal replay during rest prioritizes weakly learned information and predicts memory performance. *Nature Communications*, *9*, 3920.

Silversmith, D. B., Lemke, S. M., Egert, D., Berke, J. D., & Ganguly, K. (2020). The Degree of Nesting between Spindles and Slow Oscillations Modulates Neural Synchrony. *Journal of Neuroscience*,

40, 4673–4684.

Slotnick, S. D. (2017). *Cognitive Neuroscience of Memory*. Cambridge: Cambridge University Press.

Squire, L. R., & Dede, A. J. O. (2015). Conscious and unconscious memory systems. *Cold Spring Harbor Perspectives in Biology*, *7*, a021667.

Stages of Sleep: What Happens in a Sleep Cycle. (2021, December 2). Retrieved April 27, 2024, from Sleep Foundation website: https://www.sleepfoundation.org/stages-of-sleep

Staresina, B. P. (2024). Coupled sleep rhythms for memory consolidation. *Trends in Cognitive Sciences*, *28*, 339–351.

Staresina, B. P., Niediek, J., Borger, V., Surges, R., & Mormann, F. (2023). How coupled slow oscillations, spindles and ripples coordinate neuronal processing and communication during human sleep. *Nature Neuroscience*, *26*, 1429–1437.

Steriade, M. (2006). Grouping of brain rhythms in corticothalamic systems. *Neuroscience*, *137*, 1087–1106.

Sterpenich, V., van Schie, M. K. M., Catsiyannis, M., Ramyead, A., Perrig, S., Yang, H.-D., … Schwartz, S. (2021). Reward biases spontaneous neural reactivation during sleep. *Nature Communications*, *12*, 4162.

Stickgold, R., & Walker, M. (2005). Memory consolidation and reconsolidation: What is the role of sleep? *Trends in Neurosciences*, *28*, 408–415.

Swisher, J. D., Halko, M. A., Merabet, L. B., McMains, S. A., & Somers, D. C. (2007). Visual topography of human intraparietal sulcus. *The Journal of Neuroscience: The Official Journal of the Society for Neuroscience*, *27*, 5326–5337.

Tononi, G., & Cirelli, C. (2019). Sleep and synaptic down-selection. *The European Journal of Neuroscience*, 10.1111/ejn.14335.

Tripathy, S. P., & Öğmen, H. (2018). Sensory Memory Is Allocated Exclusively to the Current Event-Segment. *Frontiers in Psychology*, *9*, 1435.

Van Dongen, E. V., Takashima, A., Barth, M., & Fernández, G. (2011). Functional connectivity during light sleep is correlated with memory performance for face–location associations. *NeuroImage*, *57*, 262–270.

Varela, C., Kumar, S., Yang, J. Y., & Wilson, M. A. (2014). Anatomical substrates for direct interactions between hippocampus, medial prefrontal cortex, and the thalamic nucleus reuniens. *Brain Structure and Function*, *219*, 911–929.

Voss, J. L., Bridge, D. J., Cohen, N. J., & Walker, J. A. (2017). A Closer Look at the Hippocampus and Memory. *Trends in Cognitive Sciences*, *21*, 577–588.

Votaw, K. (2023). *General Psychology for Honors Students*.

Wang, J.-Y., Weber, F. D., Zinke, K., Noack, H., & Born, J. (2017). Effects of Sleep on Word Pair Memory in Children – Separating Item and Source Memory Aspects. *Frontiers in Psychology*, *8*. https://doi.org/10.3389/fpsyg.2017.01533

Weymar, M., Ventura-Bort, C., Wendt, J., & Lischke, A. (2019). Behavioral and neural evidence of enhanced long-term memory for untrustworthy faces. *Scientific Reports*, *9*, 19217.

Wierzynski, C. M., Lubenov, E. V., Gu, M., & Siapas, A. G. (2009). State-Dependent Spike-Timing Relationships between Hippocampal and Prefrontal Circuits during Sleep. *Neuron*, *61*, 587–596.

Yan, C.-G., Wang, X.-D., Zuo, X.-N., & Zang, Y.-F. (2016). DPABI: Data Processing & Analysis for (Resting-State) Brain Imaging. *Neuroinformatics*, *14*, 339–351.

Zimmer, H. D., & Ecker, U. K. H. (2010). Remembering perceptual features unequally bound in object and episodic tokens: Neural mechanisms and their electrophysiological correlates. *Neuroscience and Biobehavioral Reviews*, *34*, 1066–1079.